Publication 2834 Netherlands Institute of Ecology
Centre for Estuarine and Coastal Ecology, Yerseke,
The Netherlands

PERGAMON

Deep-Sea Research II 48 (2001) 3141–3177

DEEP-SEA RESEARCH
PART II

www.elsevier.com/locate/dsr2

Numerical modelling of the shelf break ecosystem: reproducing benthic and pelagic measurements

Karline Soetaert[a,*], Peter M.J. Herman[a], Jack J. Middelburg[a], Carlo Heip[a], Claire L. Smith[b], Paul Tett[b], Karen Wild-Allen[b]

[a] *Netherlands Institute of Ecology, Centre for Estuarine and Coastal Ecology, P.O. Box 140, 4400-AC Yerseke, The Netherlands*

[b] *Department of Biology, Napier University, Edinburgh EH10 5DT, UK*

Abstract

A coupled pelagic-benthic biogeochemical model, embedded in a turbulence-closure formulation is employed for the Goban Spur shelf-break area (northeast Atlantic). Our main objectives are to examine the impact of in situ atmospheric conditions on ecosystem dynamics, to reproduce biogeochemical distributions in the water column and the sediments, and to derive a nitrogen budget for the area. Given a data set of atmospheric forcing conditions at 3-h intervals, the model successfully explains the time evolution of the temperature field. Most biochemical water column properties are reasonably well simulated, both in timing and in magnitude. Some of the short-term variability, apparent in the data, can be reproduced, suggesting that this may result from variability in the in situ atmospheric forcing. In summer, intermittent mixing events generate increased ammonium and nitrate concentrations in the upper water column, consistent with observations. These short-term nutrient injections substantially increase euphotic zone production, mainly by stimulating new production. The model also reproduces a set of benthic nutrient profiles, measured on two occasions, both qualitatively and quantitatively. The results suggest that there is a significant variability in benthic properties.

A tentative nitrogen budget for the Goban Spur shelf break area is proposed. The sediments account for about 7% of organic nitrogen respiration; about 42% occurs in the euphotic zone, and the remaining 50% takes place in the water column below the euphotic zone. About 3% of the annual primary production of organic nitrogen is denitrified in the sediments and is replenished from lateral sources in the model. Nitrification mainly takes place in the water column below the euphotic zone (66%); sedimentary nitrification and ammonium oxidation in the euphotic zone both account for 17%. Over the year, only 55% of euphotic zone nitrogen assimilation is based on the in situ regenerated inorganic nitrogen, the remainder is mainly supplied by mixing from below the euphotic zone, either in the form of nitrate (72%) or ammonium (28%). The implications of these nitrogen pathways in the euphotic zone on the measured f-ratio are discussed.

*Corresponding author. Tel.: +31-113-577487; fax: +31-113-573616.
E-mail address: soetaert@cemo.nioo.knaw.nl (K. Soetaert).

0967-0645/01/$ - see front matter
PII: S0967-0645(01)00035-2

1. Introduction

The production and destruction of biogenic particles intimately link the cycles of many elements in the ocean and shelf seas. In the upper parts of the water column, primary producers incorporate dissolved nutrients into their biomass and produce oxygen. Subsequent consumption or degradation of these biogenic products releases inorganic nutrients and consumes oxygen. In between production and consumption of the particles, they can be relocated by mixing and/or sinking. Due to this decoupling in time and space of the incorporation and release of nutrients and oxygen, characteristic patterns in their depth distribution develop in the water column (Herbland and Voituriez, 1978), and the shape and seasonal variation of profiles may be instructive about the processes that generated them (Kiefer and Kremer, 1981).

Unfortunately, several processes can produce similar water-column distributions, and without the appropriate tools it may be difficult to decide the one in control. For instance, information on the rate and vertical extent of turbulent mixing is of prime importance for the correct interpretation of constituent distributions (Tett and Edwards, 1984). Dynamic models that link the cycles of these elements and that have a good description of the physical structure of the water mass are useful tools to interpret these signals and transform them into quantitative estimates of the fluxes themselves (e.g., Kühn and Radach, 1997; Tusseau et al., 1997).

As a part of the interdisciplinary Ocean Margin EXchange (OMEX) project, the shelf break at the Goban Spur (northeast Atlantic) was examined. A large number of cruises visited the area between 1993 and 1995, detailing the physical, biological and chemical properties of the water column and the sediments beneath. These observations indicate that substantial high-frequency variability exists in the Goban Spur shelf-break area. This natural variability and the sporadic nature of ship-board measurements make it difficult to obtain accurate annual or seasonal estimates of process rates, based on the observations alone.

It is generally thought that part of the organic matter produced on the shelf and shelf break is transported to deeper areas. The quantification of this offshore transport was one of the main research objectives of the OMEX project. Notwithstanding the emphasis in the project on lateral exchange, we decided to implement a one-dimensional model, ignoring lateral fluxes but focussing on the interaction between the water column and the sediment instead. First of all, as sediments effectuate a loss of nitrogen (by denitrification), adding a sediment model allows the estimation of a lower bound on the importance of lateral exchange of dissolved inorganic nitrogen. In addition, a one-dimensional approach for the area is supported by the results of Herman et al. (2001) who, based on the modelling of benthic profiles along the OMEX shelf-slope transect, discarded the possibility of massive off-slope transport of organic matter to the slope. Thirdly, recently, a number of numerical, dynamic models of benthic biogeochemical processes, have been developed (Boudreau, 1996; Soetaert et al., 1996a), but as far as we know, no attempt has yet been made to actually couple, in a fully dynamic sense, such a diagenetic model with a pelagic model. Therefore, the mutual impact of sediment and water column processes remains largely unaddressed.

In this paper, we describe a fully coupled physical–pelagic–benthic biogeochemical model. The pelagic model is vertically resolved, and the spatial and temporal evolution of temperature and vertical mixing intensity is described using a turbulence-closure model (Gaspar et al., 1990). The pelagic biogeochemical part is based on nitrogen and describes ammonium, nitrate, phytoplankton, zooplankton, detritus and oxygen (Smith and Tett, 2000). The vertically resolved benthic

biogeochemical model (Soetaert et al., 1996a, b) is fuelled by organic matter sinking from the overlying water column; oxygen is consumed and inorganic nitrogen returned. The model incorporates as many observations as possible from the OMEX project, both pelagic and benthic. Our goal is to arrive at a budget for the nitrogen cycle in the euphotic zone, the aphotic zone and the sediments below in the Goban Spur shelf-break area. By using real weather forcing, we investigate the extent of the observed variability in the data that can be attributed to short-term variation in local forcing.

2. Material and methods

The model resolves only the vertical dimension: the 200-m deep-water column is approximated as consisting of a stack of 30 layers with varying thicknesses, highest resolution (5 m) near the surface and bottom. The maximal thickness in the central part is 7.7 m. Similarly, the diagenetic model consists of 30 discrete layers, 1 mm thick at the sediment–water interface, subsequently increasing 20% in thickness for each consecutively deeper layer.

Pelagic model equations and boundary conditions are described in Tables 1 and 2, assuming a z-coordinate that is positive downwards. Benthic model equations, boundary conditions and parameter values are the same as in Soetaert et al. (1996a, b) and are not repeated here.

Parameter values for the present study are given in Tables 3 and 4. The structure of the model is depicted in Fig. 1.

2.1. The physical model

The physical model consists of a one-equation turbulence-closure model (Gaspar et al., 1990; Bougeault and Lacarrère, 1989). This is a relatively simple and conceptually appealing model, forecasting only the turbulent kinetic energy and involving few empirical constants. It has been successfully applied to simulate temperature evolution for oceanic conditions (e.g., Blanke and Delecluse, 1993, Hadfield and Sharples, 1996; Prunet et al., 1996).

The physical model has as prognostic variables, temperature (T, °C), horizontal water movement in two directions (U, V, $m\,s^{-1}$), and turbulent kinetic energy per unit mass (TKE, $m^2\,s^{-2}$).

The equation of the conservation of heat considers vertical turbulent diffusion and heating due to absorption of solar radiation (RAD, Table 1, first set of equations). It is assumed that 5% of the radiation (RAD) is reflected; furthermore, 54% of all penetrating solar radiation is in the infra-red band and absorbed in the upper model compartment (Smith and Tett, 2000). The remaining radiation is in the photosynthetically active radiation (PAR) and consists of a weakly-attenuated part (60%) and a strongly attenuated part (40%) (Smith and Tett, 2000). The background extinction coefficient of the weakly attenuated PAR at the Goban Spur was parameterised based on two light profiles obtained from the shelf region in winter. These light profiles below 10 m were best fit by assuming an extinction coefficient of $0.05\,m^{-1}$. The extinction coefficient of the strongly attenuated PAR was taken as $1\,m^{-1}$, such that most of it disappeared below 5 m (Smith and Tett, 2000). In addition, light is absorbed by the biota, detritus and suspended matter. At the sediment–water interface, all the remaining PAR is absorbed. At the

Table 1
The conservation equations for the physical submodel[a]

State variables	Conservation equations	Air–sea boundary	Sediment boundary
Temperature (T,°C)	$\frac{\partial T}{\partial t}=\frac{\partial}{\partial z}\left[K_z\frac{\partial T}{\partial z}\right]-\frac{1}{\rho_0 C_p}\frac{\partial I}{\partial z}$	$-K_z\frac{\partial T}{\partial z}=\frac{(1-0.05)0.54\mathbf{Rad}}{\rho_0 Cp}+\frac{Q_e+Q_s+Q_b}{\rho_0 Cp}$	$K_z\frac{\partial T}{\partial z}=\frac{I_z}{\rho_0 Cp}$ (3)
(1)	$\frac{\partial I}{\partial z}=-(1-0.05)0.46\mathbf{Rad}[pLong(k_{0long}+k_{ext})+(1-pLong)(k_{0short}+k_{ext})]\quad((Wm^{-2})m^{-1})$		
	$k_{ext}=k_{bio}(\mathrm{CPHY}+\mathrm{CZOO})+k_{det}(\mathrm{CDET_1}+\mathrm{CDET_2})+k_{sed}\mathrm{SUSP}\quad(m^{-1})$		
Horizontal velocity in x, y (u, v, m s^{-1})	$\frac{\partial u}{\partial t}-fv=-A_x\sin\left(\frac{2\pi t}{12.4\times3600}-f_x\right)+\frac{\partial}{\partial z}\left(K_m\frac{\partial u}{\partial z}\right)$	$-K_m\frac{\partial u}{\partial z}=\frac{\rho_a}{\rho_0}\mathrm{CD_{10}}\mathbf{Wind_{10}}\cos(\mathbf{Angle_{10}})\lvert\mathbf{Wind_{10}}\rvert$	$K_m\frac{\partial u}{\partial z}=BotFric\sqrt{u_1^2+v_1^2}u_1$
(2)	$\frac{\partial v}{\partial t}-fu=-A_y\sin\left(\frac{2\pi t}{12.4\times3600}-f_y\right)+\frac{\partial}{\partial z}\left(K_m\frac{\partial v}{\partial z}\right)$	$-K_m\frac{\partial u}{\partial z}=\frac{\rho_a}{\rho_0}\mathrm{CD_{10}}\mathbf{Wind_{10}}\sin(\mathbf{Angle_{10}})\lvert\mathbf{Wind_{10}}\rvert$	$K_m\frac{\partial v}{\partial z}=BotFric\sqrt{u_1^2+v_1^2}v_1$
	$f=2\times7.292\times10^{-5}\sin\left(\frac{Lat}{360}\pi\right)\quad(s^{-1})$	$\mathrm{CD_{10}}=\frac{(0.81+0.064\mathbf{Wind_{10}})}{1000}$ (–)	$u_1=\frac{u_z}{1+\frac{\sqrt{BotFric}}{\kappa}\ln\left(\frac{z}{l}\right)}\quad(m\,s^{-1})$ (4)
Turbulent kinetic energy (TKE, m^2 s^{-2})	$\frac{\partial \mathrm{TKE}}{\partial t}=K_m\left[\left(\frac{\partial u}{\partial z}\right)^2+\left(\frac{\partial v}{\partial z}\right)^2\right]-\frac{g}{\rho_0}K_z\frac{\partial \rho}{\partial z}-C_e\frac{\mathrm{TKE}^{3/2}}{l_e}+\frac{\partial}{\partial z}K_e\frac{\partial \mathrm{TKE}}{\partial z}$	$\mathrm{TKE}=C_W\frac{\rho_a}{\rho_0}\mathrm{CD_{10}}\mathbf{Wind_{10}}\mathbf{Wind_{10}}$	$\mathrm{TKE}=4u_*^2$
	$K_m=\mathrm{MIN}(VisMax, C_k l_k\sqrt{\mathrm{TKE}}+MolVisc)\quad(m^2s^{-1})$		$u_*^2=BotFric(u_1^2+v_1^2)\quad(m^2\,s^{-2})$

$$K_z = K_m Prt \ (m^2\ s^{-1})$$

$$K_e = K_m Prt \ (m^2\ s^{-1})$$

$$l_k(z_0) = MIN(l_u(z_0), l_d(z_0)) \ (m)$$

$$l_e(z_0) = \sqrt{l_u(z_0) l_d(z_0)}$$

$$\frac{g}{\rho_0} \int_{z_0}^{z_0 + l_u(z_0)} [\rho(z_0) - \rho(z)]\, dz = TKE(z_0)$$

$$\frac{g}{\rho_0} \int_{z_0 - l_d(z_0)}^{z_0} [\rho(z) - \rho(z_0)]\, dz = TKE(z_0)$$

[a] Note: Parameter values (italics) are given in Table 3; forcing functions (bold) are explained in Table 5. (1) Qe, Qs, Qb: latent, sensible heat flux and backradiation; (2): t = time in seconds; (3) lz = remaining PAR at the deepest compartment; (4): u_1 = velocity 1 m above the sediment; z = height of middle of compartment immediately above the bottom.

Table 2
Parameter values used in the physical submodel

Parameter	Value	Units	Description
κ	0.4	—	Von Karman constant
σ	5.67e−8	$W m^{-2} K^{-4}$	Stefan–Boltzmann constant
ρ_0	1025	$kg m^{-3}$	Reference water density
ρ_a	1.2	$kg m^{-3}$	Reference air density
ε^a	0.8	—	Emissivity of the air
ε^w	0.95	—	Emissivity of the water
A_x	$1.145e^{-6}$	$m s^{-2}$	M2 surface slope amplitude in E–W (x) direction
A_y	$1.259e^{-6}$	$m s^{-2}$	M2 surface slope amplitude in N–S (y) direction
BotFric	0.0025	—	Bottom quadratic friction coefficient
C_e	0.1	—	Proportionality factor between energy dissipation and $TKE^{3/2}$
CE_{10}	0.0014	—	Bulk transfer coefficient of humidity (Dalton number)
CH_{10}	0.001	—	Bulk transfer coefficient of sensible heat (Stanton number)
C_k	0.5	—	Proportionality factor between TKE and diffusivity coefficient
C_p	3994	$J kg^{-1} dgC^{-1}$	Specific heat capacity of water
C_W	3.75	—	Proportionality factor of windstress with surface TKE
Dlamp	4.0	h	Amplitude of daylength variation
Dlmean	12.0	h	Mean daylength
Dlphas	−1.5707963	—	Phase of daylength variation at reference time (1st jan)
f_x	6.95	—	M2 surface slope phase in E–W (x) direction (reference = 1st jan)
f_y	8.31	—	M2 surface slope phase in N–S (y) direction (reference = 1st jan)
g	9.81	$m s^{-2}$	Gravitational acceleration
K_{0long}	1.0	m^{-1}	Background attenuation coefficient for longer wavelength PAR (> 600 nm)
K_{0short}	0.05	m^{-1}	Background attenuation coefficient for shorter wavelength PAR
k_{bio}	$3e^{-3}$	$m^{-1}(mM m^{-3})^{-1}$	Specific extinction coefficient of biota
K_{det}	$2e^{-3}$	$m^{-1}(mM m^{-3})^{-1}$	Specific extinction coefficient of detritus
k_{sed}	$10e^{-3}$	$m^{-1}(mg m^{-3})^{-1}$	Specific extinction coefficient of sediment
Lat	49.5	°	Latitude
MinTKE	$1e^{-6}$	$m^2 s^{-2}$	Minimal turbulent kinetic energy value
MolVisc	$1e^{-6}$	$m^2 s^{-1}$	Kinematic molecular viscosity
pLong	0.4	—	Part of PAR with a long wavelength (Fast attenuation coefficient k_{0Long})
Prt	1	—	Turbulent Prandtl number
RADamp	112.94	$W m^{-2}$	Amplitude of solar radiation variation
RADmean	133.55	$W m^{-2}$	Mean solar radiation
RADphas	−1.396	—	Phase of daily radiation at reference time (1st jan)
RADRANamp	320	$W m^{-2}$	Amplitude of stochastic light component
Sal	35.5	PSU	Salinity of the water column
TefoldRAD	1.61	d^{-1}	e-folding decay time scale of random light comp
VisMAX	1.0	$m^2 s^{-1}$	Maximal vertical diffusivity/viscosity

air–sea interface, heat is transferred by conduction, by evaporation, by incoming short-wave and by back-radiation. Sensible and latent heat fluxes are estimated using the bulk transfer functions (Blanc, 1985). The net long-wave back-radiation is estimated as in Edinger et al. (1968).

The equations of conservation of momentum takes into account the Coriolis term, tidal forcing and turbulent exchange (Table 1, second set of equations), as in Sharples and Tett (1994). At the

Table 3
The conservation equations used in the biogeochemical pelagic model[a]

State variables	Conservation equations	Air–sea boundary	Sediment boundary
Phytoplankton C (CPHY, mmol $C\,m^{-3}$) (*)	$\frac{\partial CPHY}{\partial t} = \frac{\partial}{\partial z}\left[K_z \frac{\partial CPHY}{\partial z}\right] - w_{PHY}\frac{\partial CPHY}{\partial z} + \text{Growth} - PHY_{mort} - ZOO_{graz}$	$-K_z\frac{\partial CPHY}{\partial z} + w_{PHY}CPHY = 0$	Flux $= w_{PHY}CPHY$

$$w_{PHY} = wPHYMin + (wPHYMax - wPHYMin)\frac{MaxNCrPHY - NCrPHY}{MaxNCrPHY - MinNCrPHY} \quad (m\,d^{-1})$$

$$\text{Growth} = \text{MIN}\left[(MaxQuantI\,\text{ChlCrPHY} - Resp)(1 - Prod\text{Resp}),\ MuMax\left(1 - \frac{MinNCrPHY}{NCrPHY}\right)\right] f(T)\text{CPHY} \quad (mmol\,C\,m^{-3}\,d^{-1})$$

$$\text{PHYmort} = rPHYmort\,f(T)\text{CPHY} \quad (mmol\,C\,m^{-3}\,d^{-1})$$

$$\text{Zoograz} = Maxgraz\,f(T)\frac{CPHY}{CPHY + ksGraz}\text{CZOO} \quad (mmol\,C\,m^{-3}\,d^{-1})$$

$$\text{ChlCrPHY} = \text{NCrPHY}\left[MinChlNr + (MaxChlNr - MinChlNr)\frac{(NCrPHY - MinNCrPHY)}{(MaxNCrPHY - MinNCrPHY)}\right] \quad (mg\,Chl\,mmol\,C^{-1})$$

$$\text{NCrPHY} = \frac{NPHY}{CPHY} \quad (mmol\,N\,mmol\,C^{-1})$$

Table 3 (*continued*)

State variables	Conservation equations	Air–sea boundary	Sediment boundary
	$f(T) = e^{LN(q10)\frac{T-20}{10}}$ (–) (1)		
Phytoplankton N (NPHY, mmol N m^{-3})	$\frac{\partial NPHY}{\partial t} = \frac{\partial}{\partial z}\left[K_z \frac{\partial NPHY}{\partial z}\right] - w_{PHY}\frac{\partial NPHY}{\partial z} + NHuptake + NOuptake - (PHYmort + ZOOgraz)NCrPHY$	$-K_z\frac{\partial NPHY}{\partial z} + w_{PHY}NPHY = 0$	Flux = w_{PHY}NPHY
	$NOuptake = NOuMax\, f(T)\left(1 - \frac{NCrPHY}{MaxNCrPHY}\right)\frac{NOs}{NOs + ksNOs}\frac{kinNH3}{NHs + kinNH3}CPHY \quad (mmol\, N\, m^{-3}\, d^{-1})$		
	$NHuptake = NHuMax\, f(T)\left(1 - \frac{NCrPHY}{MaxNCrPHY}\right)\frac{NHs}{NHS + ksNHs}CPHY \quad (mmol\, N\, m^{-3}\, d^{-1})$		
Detrital C (CDET mmol C m^{-3}) (i = 1, 2)	$\frac{\partial CDETi}{\partial t} = \frac{\partial}{\partial z}\left[K_z\frac{\partial CDETi}{\partial z}\right] - w_{DETi}\frac{\partial CDETi}{\partial z} - CMinrate_i + \left[(1 - AssZOO)ZOOgraz + \frac{1 - AssZOO}{1 - EffZoo\, AssZoo}ZOOmort + PHYmort\right]p_i$ (2)	$-K_z\frac{\partial CDETi}{\partial z} + w_{Deti}CDETi = 0$	Flux = w_{DETi}CDETi
	$CMinrate_i = CDetMax\, f(T)\left[1 - \frac{MinNCrDet}{NCeDet_i}\right]\frac{OX}{OX + ksO2Deg}CDETi \quad (mmol\, C\, m^{-3}\, d^{-1})$		

$$\mathrm{NCrDET_i} = \frac{\mathrm{NDETi}}{\mathrm{CDETi}} \quad (mmol\ N\ mol\ C^{-1})$$

$$\mathrm{ZOOmort} = MortZoo\ \mathrm{CZOO}^2\ \mathrm{f(T)} \quad (mmol\ C\ m^{-3}\ d^{-1})$$

Detrital N (NDET mmol N m^{-3})

$$\frac{\partial \mathrm{NDETi}}{\partial t} = \frac{\partial}{\partial z}\left[\mathrm{K_z}\frac{\partial \mathrm{NDETi}}{\partial z}\right] - w_{DETi}\frac{\partial \mathrm{NDETi}}{\partial z} - \mathrm{NMinrate_i} + \left\{NCrZOO\left[(1 - AssZOO)\mathrm{ZOOgraz} + \frac{1 - AssZOO}{1 - EffZooAssZoo}\mathrm{ZOOmort}\right] + \mathrm{NCrPHY}\ PHYmort\right\}\mathrm{p_i}$$

$$-\mathrm{K_z}\frac{\partial \mathrm{NDETi}}{\partial z} + w_{Deti}\mathrm{NDETi} = 0$$

$$\mathrm{Flux} = w_{DETi}\mathrm{NDETi}$$

$$\mathrm{NMinrate_i} = \mathrm{NDetMax\ f(T)}\left[1 - \frac{MinNCrDet}{\mathrm{NCrDet_i}}\right]\mathrm{NDETi} \quad (mmol\ N\ m^{-3}\ d^{-1})$$

Zooplankton C (CZOO, mmol C m^{-3})

$$\frac{\partial \mathrm{CZOO}}{\partial t} = \frac{\partial}{\partial z}\left[\mathrm{K_z}\frac{\partial \mathrm{CZOO}}{\partial z}\right] - w_{\mathrm{ZOO}}\frac{\partial \mathrm{CZOO}}{\partial z} + EffZOO\ AssZOO\ \mathrm{ZOOgraz} - \mathrm{ZOOmort}$$

$$-\mathrm{K_z}\frac{\partial \mathrm{CZOO}}{\partial z} + w_{\mathrm{ZOO}}\ \mathrm{CZoo} = 0$$

$$\mathrm{K_z}\frac{\partial \mathrm{CZOO}}{\partial z} - w_{ZOO}\ \mathrm{CZOO} = 0$$

Suspended matter (SUP, mg m^{-3})

$$\frac{\partial \mathrm{SUSP}}{\partial t} = \frac{\partial}{\partial z}\left[\mathrm{K_z}\frac{\partial \mathrm{SUSP}}{\partial z}\right] - w_{SUSP}\frac{\partial \mathrm{SUSP}}{\partial z}$$

$$-\mathrm{K_z}\frac{\partial \mathrm{SUSP}}{\partial z} + w_{SUSP}\ \mathrm{SUSP} = 0$$

$$\mathrm{K_z}\frac{\partial \mathrm{SUSP}}{\partial z} - w_{SUSP}\ \mathrm{SUSP} = fRate(Susp_0 - \mathrm{SUSP})$$

Nitrate (NOs, mmol N m^{-3})

$$\frac{\partial \mathrm{NOs}}{\partial t} = \frac{\partial}{\partial z}\left[\mathrm{K_z}\frac{\partial \mathrm{NOs}}{\partial z}\right] - \mathrm{NOuptake} + \mathrm{Nitrif}$$

$$-\mathrm{K_z}\frac{\partial \mathrm{NHs}}{\partial z} = 0$$

$$\mathrm{K_z}\frac{\partial \mathrm{NHs}}{\partial z} = f(Diagen)$$

$$\mathrm{Nitrif} = NHsOxMax\ \mathrm{f(T)NHs}\frac{\mathrm{OX}}{\mathrm{OX} + ksO2Nit} \quad (mmol\ N\ m^{-3}\ d^{-1})$$

Table 3 (*continued*)

State variables	Conservation equations	Air–sea boundary	Sediment boundary
Ammonium (NHs, mmol C m^{-3})	$\frac{\partial NHs}{\partial t} = \frac{\partial}{\partial z}\left[K_z \frac{\partial NHs}{\partial z}\right] - NHuptake - Nitrif + \sum_i NMinrate_i + NCrZOO\left[(1 - EffZoo)AssZoo\ ZOOgraz + \frac{(1 - EffZoo)AssZoo}{1 - EffZoo\ AssZoo} ZOOmort\right] + \gamma$ (3)	$-K_z \frac{\partial NOs}{\partial z} = 0$	$K_z \frac{\partial NOs}{\partial z} = f(Diagen)$
Oxygen (OX, mmol O m^{-3})	$\frac{\partial OX}{\partial t} = \frac{\partial}{\partial z}\left[K_z \frac{\partial OX}{\partial z}\right] + ONr(NOuptake - Nitrif) + OCr\left[Growth - \sum_i CMinrate_i - (1 - effZoo)AssZoo\ ZOOgraz - \frac{(1 - EffZoo)AssZoo}{1 - EffZoo\ AssZoo} ZOOMort\right]$	$-K_z \frac{\partial OX}{\partial z} = f(W_{10})(SatOX - Ox) + O2_{inj}$ (5)	$K_z \frac{\partial OX}{\partial z} = f(Diagen)$
		$f(W_{10}) = 0.78\sqrt{W_{10}} - 0.317W_{10} + 0.0372W_{10}^2$ (–)	
		$SatOX = f(T, Sat)$ (4) (mmol O m^{-3})	

[a] Note: *Parameter values* (italics) are given in Table 4. (1) T is the water temperature, w_{10} is the wind speed 10 m above the sea surface (forcing function), I is photosynthetically active radiation (See Table 1); (2) i = 1 is the fast sinking fraction; i = 2 is the slowly sinking faction; $p_1 = pFastSink$, $p_2 = 1 - p$; (3) γ is a function used to conserve mass in the stochiometric calculations (when exchanging between pools with different N/C ratios); (4) saturated oxygen concentration is calculated from Weiss (1970); (5) oxygen injection as in Thorpe (1984).

Table 4
Parameter values used in the biochemical part of the model

Parameter	Value	Units	Description
PELAGIC			
AssZOO	0.7	—	Fraction of phytoplankton intake assimilated by zooplankton
CDETMax	0.29	d^{-1}	Maximal degradation rate of detrital C at 20°C
cMortPHY	0.03	d^{-1}	Daily mortality rate of phytoplankton at 20°C
EffZOO	0.25	—	Part of the assimilated food of Zooplankton used for growth
fRate	0.5	d^{-1}	Benthic suspended matter input rate
KsGraz	5.0	mmol C m^{-3}	Half-saturation concentration of zooplankton grazing on phytoplankton
KsNHs	0.3	mmol NH_3-N m^{-3}	Half-saturation concentration of NH_3 uptake phytoplankton
KsNOs	0.3	mmol NO_3-N m^{-3}	Half-saturation concentration of NO_3 uptake phytoplankton
KsO2Deg	3.0	mmol O_2 m^{-3}	Half-saturation concentration of O_2 limitation detrital respiration
KsO2Nit	1.0	mmol O_2N m^{-3}	Half-saturation ccncentration of O_2 limitation nitrification
MaxChlNr	2.0	mg Chl mol N^{-1}	Maximal chlorophyll/nitrogen ratio of phytoplankton
MaxGraz	5.0	d^{-1}	Maximum grazing rate of zooplankton at 20°C
MaxNCrPHY	0.2	mol N mol C^{-1}	Maximal nitrogen/carbon ratio of phytoplankton
MaxQuant	0.4	mmol C (mg Chl d W $m^{-2})^{-1}$	Maximum quantum yield
MinChlNr	1.0	mg Chl mol N^{-1}	Minimal chlorophyll/nitrogen ratio of phytoplankton
MinNCrDET	0.116	mol N mol C^{-1}	Minimal nitrogen/carbon ratio of detritus
MinNCrPHY	0.05	mol N mol C^{-1}	Minimal nitrogen/carbon ratio of phytoplankton
MortZOO	0.45	$(mMC\,m^{-3})^{-1}\,d^{-1}$	Quadratic zooplankton mortality term
MuMax	3.0	d^{-1}	Maximal specific growth rate of phytoplankton at 20°C
NCrZOO	0.15	mol N mol C^{-1}	Nitrogen/carbon ratio of zooplankton
NDETMax	0.33	d^{-1}	Maximal degradation rate of detrital N at 20°C
NHsOXMax	0.05	d^{-1}	Maximal ammonium oxidation rate at 20°C
NhuMax	1.0	mmol NH_3-N.mmol C d^{-1}	Maximal ammonium uptake rate by phytoplankton at 20°C
NouMax	0.4	mmol NO_3-N.mmol C d^{-1}	Maximal nitrate uptake rate by phytoplankton at 20°C
Ocr	1.0	mol O_2.mol C^{-1}	Oxygen to carbon ratio
Onr	2.0	mol O_2 mol N^{-1}	Oxygen needed to convert ammonium to nitrate
pFastSink	0.14	—	Fraction of detrital production that is fast sinking
ProdResp	0.25	—	Part of net primary production that is used for respiration
Q10	2.0	—	Q10 for temperature dependent rates
Resp	0.05	d^{-1}	Respiration rate of phytoplankton
$Susp_0$	0.05	mg m^{-3}	Concentration of suspended matter above the bottom
w_{DET1}	100	m d^{-1}	Sinking speed of the fast sinking detrital fraction (CDET1, NDET1)
w_{DET2}	0.5	m d^{-1}	Sinking speed of the slow sinking detrital fraction (CDET2, NDET2)
wPHYMax	5.0	m d^{-1}	Maximal Sinking rate of phytoplankton
wPHYMin	0.5	m d^{-1}	Minimal Sinking rate of phytoplankton
w_{SUSP}	100	m d^{-1}	Suspended matter sinking speed
wZOO	0.0	m.d^{-1}	Zooplankton sinking speed
DIAGENETIC			
Φ_0	0.853	—	Porosity at sediment–water interface
Φ_∞	0.72	—	Porosity at depth
Φ_{coeff}	0.25	cm	Coefficient for exponential porosity decline
Db	0.004	$cm^2.d^{-1}$	Sediment mixing coefficient
w	0.000011	cm.d^{-1}	Advection rate

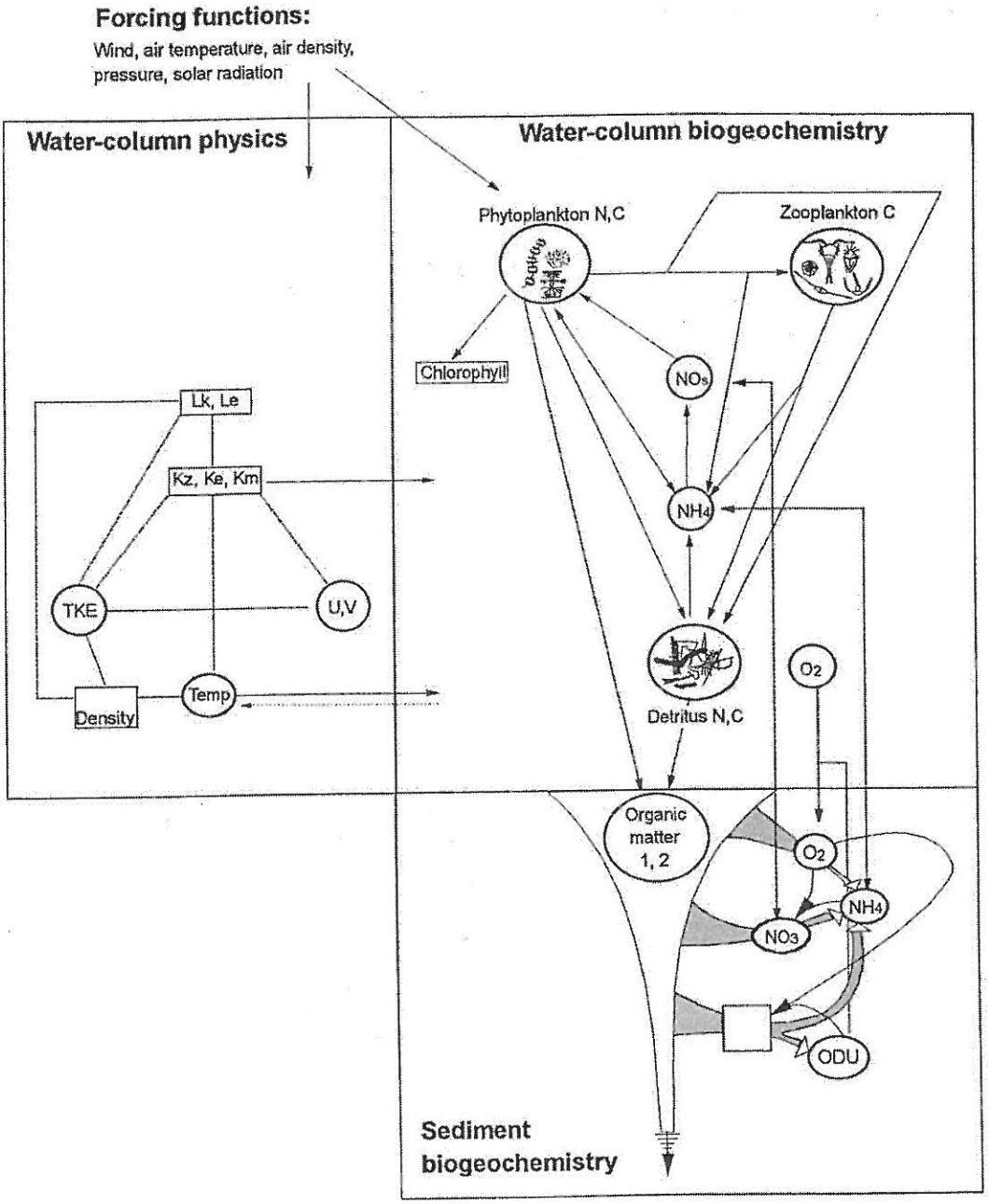

Fig. 1. Model structure, encompassing the physical submodel, the biogeochemical pelagic and diagenetic model. Circles denote state variables, related quantities are in rectangles. (Empty box = not modelled).

sea surface, the model is forced by wind stress; the surface drag coefficient (CD_{10}) depends on wind speed and is calculated from a bulk aerodynamic formula (Smith, 1988). At the sea floor, the frictional stress is computed from current velocities 1 m above the bottom; the latter is estimated using the nearest computed velocities and an assumed logarithmic profile.

Mass-specific turbulent kinetic energy (TKE) is generated or destroyed by buoyancy and shear stress, and redistributed in the water column through turbulent mixing (Table 1, third set of equations). The dissipation rate is parameterised according to Kolmogorov (1942, in Gaspar et al., 1990), assuming a turbulent length scale l_e. At the sediment–water interface, the turbulent kinetic energy is prescribed with a bottom-stress expression, as in Blumberg and Mellor (1987). A stress condition is also applied at the air–sea interface (Gaspar et al., 1990).

Density is calculated from temperature and salinity (the latter is a constant) using the standard formula (Millero and Poisson, 1981), but ignoring coefficients of higher order than T^3.

The turbulent viscosity (K_m), the turbulent diffusivity (K_z) and the turbulent mixing coefficient for turbulent kinetic energy (K_e) are calculated as a function of the turbulent kinetic energy and a turbulent length scale l_k (Table 1). It is assumed that all turbulent mixing coefficients are equal (turbulent Prandtl numbers, Prt are equal to unity).

The two length scales (relating to dissipation, l_e, and mixing, l_k) are simple functions of two primary length scales, defined as the distances travelled upward (l_u) or downward (l_d) by a fluid particle while converting all its original TKE into potential energy. The enhanced mixing often observed over a shelf-break area is parameterised by including a minimal value below which the turbulent kinetic energy per unit mass may not fall ($\text{MinTKE} = 1 \times 10^{-6}\,\text{m}^2\,\text{s}^{-2}$). This value accords with that used by Gaspar et al. (1990).

2.2. The pelagic biochemical model

The basis of the pelagic biochemical model is a model of unbalanced phytoplankton growth (Tett, 1998; Smith and Tett, 2000). In this model, carbon and nitrogen assimilation is decoupled (in time and space), resulting in a variable N:C ratio. Nitrogen assimilation reflects the luxury uptake of DIN, whereas carbon assimilation (photosynthesis) is synonymous with growth. Nitrogen uptake increases at lower N:C ratios and is unaffected by the light intensity (it can proceed in the dark, e.g., Laws and Wong, 1978), whereas photosynthesis increases with higher N:C ratios. Since this model takes into account the physiological status of the algae (as reflected in the N:C ratio), a more realistic response of phytoplankton dynamics with respect to short-term changes in the abiotic environment is achieved. Therefore, such a model is better suited to test the impact of short-term physical forcing on ecosystem dynamics than when using the more commonly used balanced-growth models, where N- and C-assimilation occurs concurrently.

Light-limited carbon assimilation is expressed by a quantum efficiency formulation (Sharples and Tett, 1994), while nitrogen incorporation follows Droop kinetics (Tett and Droop, 1988). Ammonium inhibition of nitrate uptake is modelled with a hyperbolic equation. Phytoplankton respiration assumes a basal rate and a production-dependent term. A fixed but small fraction of the phytoplankton dies off per day. The chlorophyll-to-carbon ratio of the phytoplankton depends on their internal N:C ratio. The higher this ratio (more light-limited), the higher the chlorophyll-to-carbon ratio.

In addition to the algal growth model, is a dynamic description of the zooplankton (Henderson and Steele, 1995) and of four detrital pools: detrital nitrogen and carbon, both subdivided into two sinking classes. Dissolved inorganic nitrogen consists of nitrate and ammonium, whereas oxygen is also modelled as an additional constraint on the autotrophic/heterotrophic processes

and allows the coupling with the sediment model (Fig. 1). Suspended matter is included because of its impact on the penetration of light.

Zooplankton graze on phytoplankton only; part of the food is not assimilated and enters the detrital pools; part of the assimilated food is respired. A quadratic mortality term accounts for non-modelled higher predators; this mortality term is the input to an infinite series of higher predators that have the same growth and assimilation efficiency as the zooplankton itself (Fasham et al., 1990). To a certain extent this term also accounts for recycling within the zooplankton compartment, i.e., larger zooplankton grazing on smaller zooplankton.

Detrital matter is split up in a nitrogen and carbon pool, and the mineralisation rate of detritus depends on its N : C ratio; the larger the ratio, the higher is the oxidation rate. Organic nitrogen decays faster than carbon; hence, the N : C ratio (and therefore the degradability) of the detritus decreases with ageing. Without a functional aggregation model or data, detrital sinking is described in a simple way by distinguishing two classes for each detrital pool: one sinks rapidly ($100\,m\,d^{-1}$) and one sinks slowly ($0.5\,m\,d^{-1}$). For both sinking classes, the parameterisation of the mineralisation rate is the same. The ammonium produced by biotic respiration and mineralisation processes is slowly oxidised to nitrate, a process that is described first-order in ammonium and limited by oxygen (Michaelis–Menten equation), similar to sediment nitrification, but with a much smaller rate constant. All the model equations depend on temperature, with a doubling of the rates for every 10°C of increase in temperature (Q_{10} formulation).

Net oxygen flux at the air–sea interface depends on the difference in partial pressure of oxygen in air and the surface water, and a transfer coefficient (Piston velocity), which is a function of wind speed and sea-surface temperature, according to the simple formulation of Thomann and Mueller (1987). In addition, air injection is parameterised using the formula of Thorpe (1984) and Wallace and Wirick (1992). None of the other biogeochemical state variables is exchanged across the air–sea interface.

Vertical mixing of pelagic constituents is described as diffusion with a turbulent diffusivity coefficient calculated as above. Particles may have a vertical sinking speed, which is either constant (detritus, suspended matter) or varies with the internal N : C ratio (phytoplankton).

2.3. *The sediment model*

The sediment biogeochemistry is described by the diagenetic model of Soetaert et al. (1996a, b), and includes the time evolution of two organic matter fractions (with different N : C ratios and degradability), oxygen, nitrate, ammonium, and other reduced substances (called 'oxygen demand units', ODU) (Fig. 1). The oxidation of the two benthic detritus fractions uses a sequence of oxidants of which only oxygen and nitrate are explicitly modelled. Organic matter mineralisation is first-order with respect to the organic matter concentration. The oxic mineralisation is limited by the oxygen concentration (Monod term), while the denitrification is limited by nitrate and inhibited by oxygen (Monod, 1-hyperbolic, respectively). The anoxic mineralisation processes are inhibited by both oxygen and nitrate (1-hyperbolic). The nitrification, the oxidation of other reduced substances, and solid deposition of reduced substances below the bioturbation zone are also described. All these processes are embedded in the sediment variant of the advection-diffusion equation, which in essence includes the effects of sediment compaction and tortuosity (Berner, 1980; Boudreau, 1996).

2.4. Coupling the submodels

Coupling of pelagic and the diagenetic models is performed such that total mass is conserved. Modelled concentrations of dissolved oxygen, nitrate and ammonium in the lower layer of the water column are used as boundary conditions for the diagenetic model. Organic matter, arriving at the sea floor, is distributed over the two benthic detritus fractions in proportions determined by their N:C ratios. Oxygen, nitrate and ammonium fluxes calculated by the diagenetic model are then used to adjust the rate of change of the equivalent substances in the lowermost pelagic compartment. The (very small) outward flux of the other reduced substances (ODUin Soetaert et al., 1996a, b) is assumed to be immediately oxidised upon entering the water column.

The biogeochemistry of the water column affects the physics through the modulation of the light and heat budgets due to the absorption of solar radiation by the biota and detritus, which slightly changes the temperature distribution and mixing characteristics. The physical submodel impacts the biogeochemistry by redistributing biogeochemical constituents in the water column, based on the temporally and spatially variable eddy diffusivity. In addition, most biogeochemical rates are temperature dependent.

2.5. Lateral exchange

Due to sedimentary denitrification, some nitrogen is lost from the system (mainly as N_2 gas). In a one-dimensional model, this nitrogen must be returned, to conserve mass and to allow multi-year simulations. We added the denitrified nitrogen as nitrate, at a rate proportional to the current standing stock, thus mimicking lateral advection. As such the total nitrogen inventory in the model was constant. Other scenarios of nitrogen re-supply were tested, (i.e. constant throughout the year, uniform with depth), but produced only marginal differences. It should be noted that the estimate of lateral input thus obtained may be a minimal estimate because we have ignored the export of organic nitrogen.

2.6. Implementation

Numerical approximation of the diagenetic equations is described in Soetaert et al. (1996a, b).

In the pelagic submodel, scalars and velocities are defined in the centre of compartments, turbulent mixing coefficients (K_m, K_z) and mass specific turbulent kinetic energy are defined at the compartment interfaces. Time stepping is done using explicit Euler integration, except for turbulent mixing and the momentum equation, which is solved by a two-time step implicit method (Kurihara, 1965), and the Kolmogorov term of the TKE equation, which is solved implicitly (after linearizing). Finite differencing is centred in space for the diffusive terms, while the sinking terms are solved by means of backward differences. The pelagic model alone can be run with a time step of 0.125 h, where the fully coupled model (including the dynamic diagenetic model) requires a time step about 10 times smaller. The model was implemented on a personal computer in FORTRAN. The model runs from 28-06-93 (day 179) until 30-06-95 (day 908). All model output is averaged over a day.

2.7. Model forcing

The external forcings are imposed as temporal variations in wind ($m\,s^{-1}$), atmospheric pressure (Pa), specific air humidity (dimensionless), air temperature (°C), air density ($kg\,m^{-3}$), and solar radiation ($W\,m^{-2}$). Except for the latter quantity, these forcing functions consist of 3-h averages, 4 m above the sea surface at K2 Buoy (48°42′N, 12°24′W). They were obtained from the UK Meteorological Office (1-06-1993 until 30-06-1995) and converted to 10 m above the sea surface, using a method outlined in Smith (1988), assuming neutrally buoyant conditions. Missing data were interpolated as follows: when the gap was less than 3 days, the data were linearly interpolated. When the gap was larger, a time series was created. This series consisted of a sine function (period of 1 year) to which random noise was added; the parameters of these series were derived from the available data set. The largest gap in the data was for the whole of December 1994 (day 700–730).

Unfortunately, we did not possess light field data with similar temporal resolution. Hence, for mean daily radiation, we used a sine function (Clarke, 1986) to which a random perturbation was added (Table 5). The daily cycle of solar radiation is calculated as a function of the time of day, with a daylength varying from 8 to 16 h (also a sine function; see Table 5).

2.8. Initial conditions

The initial condition for the temperature field was obtained from a station at 49°57′N and 11°5′W, (201-m water depth) sampled on 28 June 1993 (day 179). Starting conditions for the horizontal velocity profiles were obtained first by running the model for one year and using the final velocities thus calculated as starting values for the subsequent runs. Initial turbulent kinetic energy was a uniform profile with a value of $1 \times 10^{-6}\,m^2\,s^{-2}$. Starting conditions for oxygen, nitrate and ammonium were measured concentrations at a station at 49° 50′N and 11°W (180-m water depth), sampled on 28 June 1993 (day 179).

Initial concentrations for the substances in the diagenetic model were obtained as the steady-state solution, based on yearly averaged deposition fluxes and bottom-water conditions (see Soetaert et al., 1996a for more details for calculating the steady-state solution).

2.9. Data used for the calibration

The Goban Spur shelf break area was delimited as the area between 48 and 51°N, 8 and 13°W, with a water depth varying between 150 and 250-m . A variety of measurements were used for the evaluation of model performance and model calibration. Some were taken in raw form, from the OMEX database (Lowry et al., 1997), while other data sets required transformation before they were converted into a usable quantity. Measurements of the f-ratio were used as an *a posteriori* check on model performance.

Surficial concentrations of chlorophyll (0–5 m), nitrate (0–5 m), ammonium (0–5 m), oxygen (0–5 m) and microzooplankton (0–10 m), mean deep concentrations (> 150 m) of nitrate, ammonium and oxygen, and the mean oxygen concentration in the upper 100 m of the water column were obtained directly from the database. Temperature at various water depths was available from CTD casts.

Table 5
Forcing functions[a]

Wind10	Windspeed, 10 m above the sea surface, time series (K2 Buoy)
Angle 10	Wind angle, time series (K2 Buoy)
$\mathbf{T_{10}}$	Air temperature, 10 m above the sea surface, time series (K2 Buoy)
$\mathbf{q_{10}}$	Relative humidity, 10 m above the sea surface, time series (K2 Buoy)
Press	Sea surface pressure, time series (K2 Buoy)
Rad	Solar radiation, calculated as follows:

$$\mathrm{Rad} = \mathrm{Max}(0, \mathrm{RadMax}\, f(\mathrm{Hour}))$$

$$\mathrm{RadMax} = (\mathrm{DayRad} + \mathrm{RadRan})\pi\frac{12}{\mathrm{DayLength}}$$

$$\mathrm{DayRad} = RadMean + RadAmp \sin\left(\frac{2\pi}{365}t + RadPhas\right) \quad (1)$$

$$\mathrm{DayLength} = DLMean + DLAmp \sin\left(\frac{2\pi}{365}t + DLPhas\right) \quad (1)$$

$$f(\mathrm{Hour}) = \sin\left(\frac{2\pi}{24}Hour\frac{12}{\mathrm{DayLength}}\right) \quad (2)$$

$$\mathrm{RadRan} = \mathrm{RadRan} * \left(1 - \frac{1}{TeFoldRAD}\right) \frac{\mathrm{DayRad}}{RADMean + RADAmp} RADRANAmp[RANDOM() - 0.5] \quad (3)$$

[a]Note: (1) t is in days; (2) Hour is the hour of the day; (3) updated once per day.

Flux data used to constrain the model consisted of euphotic zone primary production estimates (Joint et al., 1994; Joint and Rees, 1995) and sediment community oxygen demand estimates for the sediment below (Duineveld et al., 1997). Sediment oxygen, nitrate and ammonium profiles (Lohse et al., 1998) were available from two sampling occasions. All other data were derived indirectly by curve-fitting primary data as described below.

2.9.1. The mixed layer depth, position and shape of the nitracline

In order to compare the modelled and observed mixed-layer depth, we estimated it by fitting the density profiles with a two-layer model, consisting of a surficial mixed layer (depth MLD) with constant density (ρ_0), below which the density increases to density ρ_∞ according to an exponential function (Fig. 2a). The nitrate profiles could be fitted with a similar model, defined by four parameters: the nitrate concentration in the mixed layer (N_0), the depth of the nitracline (z_n), the nitrate concentration at depth (N_∞), and the coefficient of increase (c) (Fig. 2b). The significance of the fit with respect to a model with constant density or nitrate concentration was tested by

means of an F-test (Sokal and Rohlf, 1995). In all but two cases for nitrate was the more complex model significantly better than the constant nitrate concentration model.

2.9.2. Chlorophyll and ammonium maximum depth and mean concentration

The position of the chlorophyll maximum, the mean chlorophyll concentration in the upper 100 m of the water column, the position of the ammonium peak, and the depth-averaged ammonium concentration were obtained from non-linear fitting of the profiles with a shifted Gaussian distribution, as outlined in Platt et al. (1988). An example of such a fit to an ammonium profile is given in Fig. 2c. It was tested if the Gaussian fit was significantly better than an exponentially decreasing concentration profile using an F-test (Sokal and Rohlf, 1995). In all but five cases for the ammonium profile was the Gaussian model significantly the best. Chlorophyll concentrations based on CTD profiles provided sufficient vertical resolution and did not require statistical fitting.

3. Results

3.1. Physics

In the Gaspar et al. (1990) model, there are two tuneable parameters, relating to the dissipation rate (the proportionality factor C_e) and to the calculation of the mixing coefficients (proportionality factor C_k). Typical values for these quantities are in between 0.1 and 0.5 for C_k and in between 0.1 and 0.7 for C_e (e.g., Gaspar et al., 1990; Martin and Delhez, 1994). We performed several model runs with contrasting combinations of these parameters and compared observed and modelled temperatures at several depths in the water column.

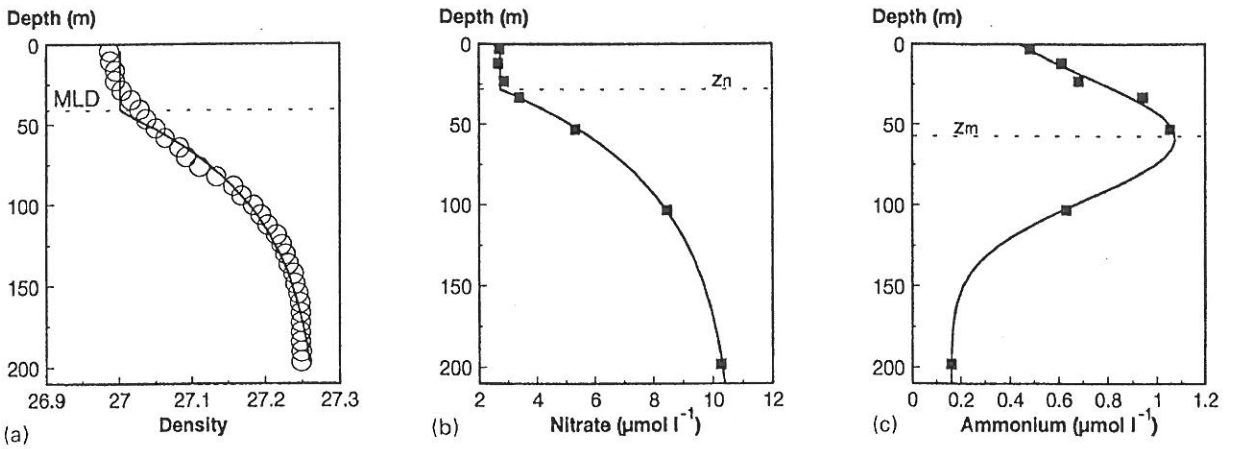

Fig. 2. An example of non-linear fits used to estimate mixed layer depth, MLD (a); depth of the nitracline, (z_n) and mean nitrate concentration (b) and the position of the ammonium maximum, (z_m) and mean ammonium concentration (c).

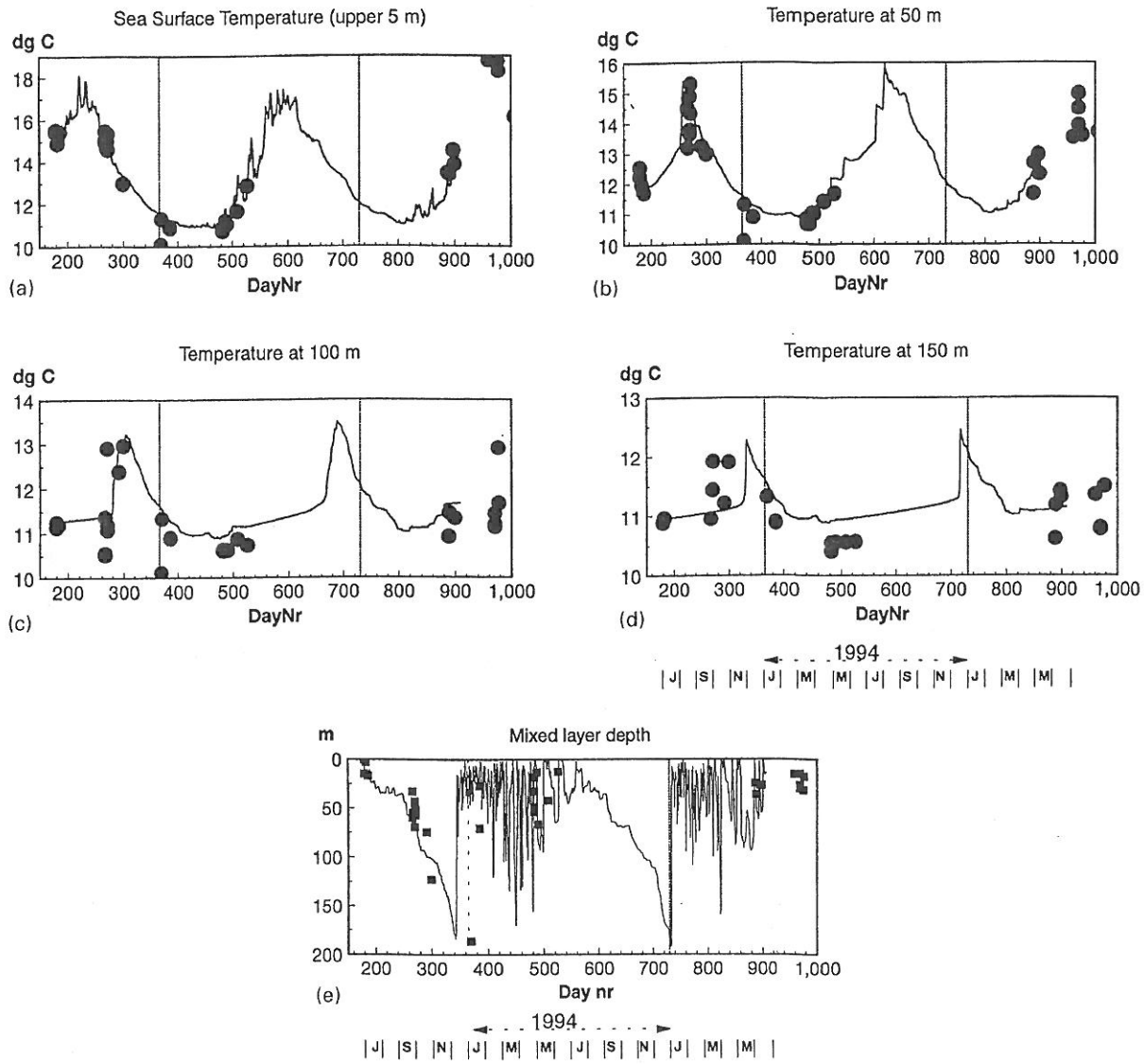

Fig. 3. Fit of modelled and observed temperature (a, 0–5; b, 50; c, 100; and d, 150 m) and fit of modelled and observed mixed layer depth (e).

The best correspondence between modelled and observed data is obtained when proportionality factors typical for shelf regions are used ($C_e = 0.1$, $C_k = 0.5$; see Fig. 3). These parameters best reproduce the sudden rise in temperature at 100 m depth in fall (Fig. 3c), although the winter temperature at 100–150-m depth may be somewhat overestimated (Fig. 3d). These model settings result in a water column that is the most vigorously mixed.

The shape of the predicted density field was further assessed by comparing the model-generated mixed layer depth (see above) with estimates obtained by fitting the data. The onset and magnitude of destratification in fall is reasonably well reproduced, although it seems to appear a few weeks too early (Fig. 3e; day 250–300). From December till April–May (day 350–500, 730–820), the upper part of the water column is highly turbulent and alternatingly stratifies and

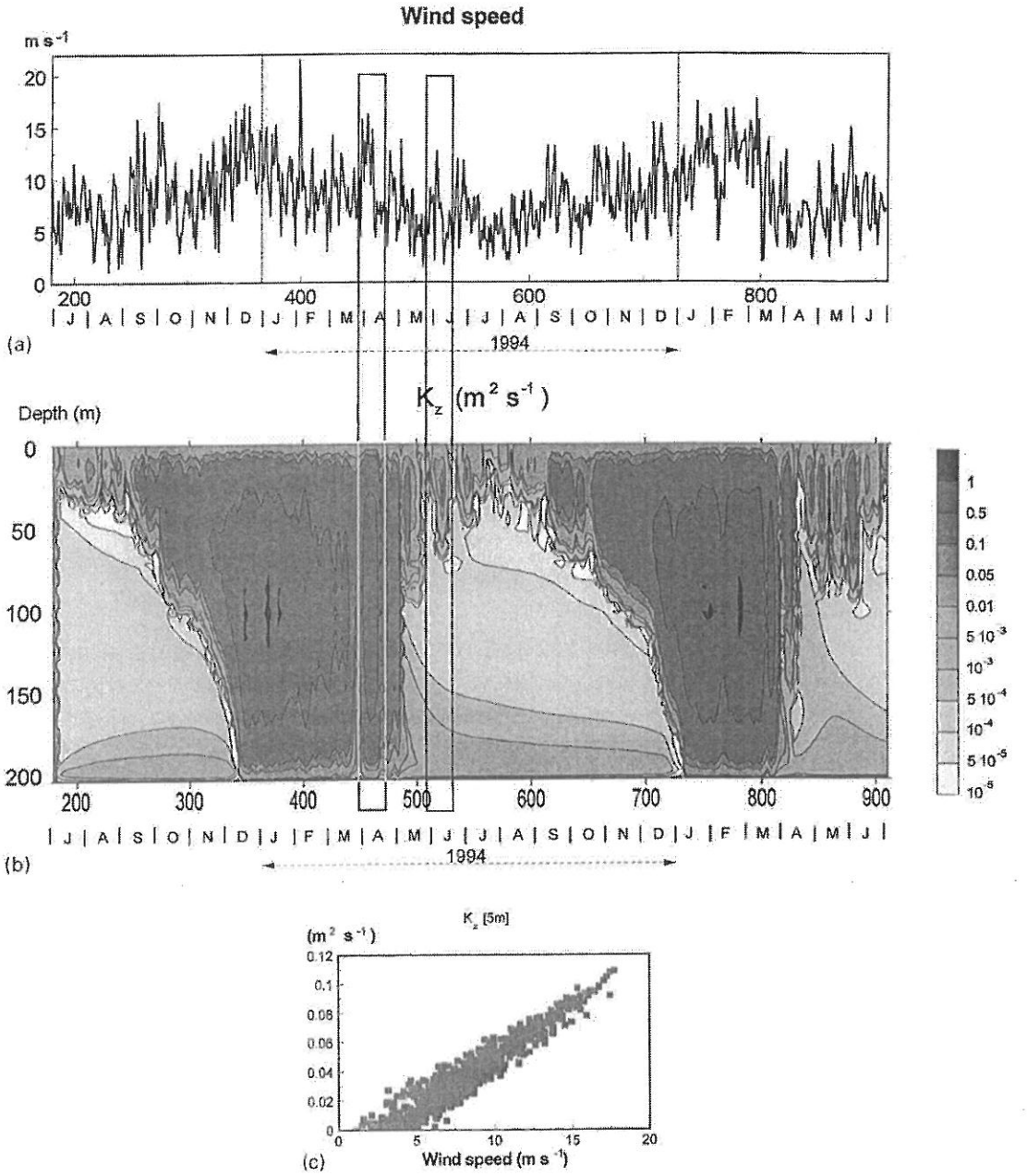

Fig. 4. a. Wind speed used as a forcing function ($m\,s^{-1}$). b. Spatio-temporal evolution of the vertical diffusivity coefficient (K_z, $m^2\,s^{-1}$). Emphasised here are two wind-driven mixing events. c. Relationship between wind speed and the modelled diffusivity coefficient at 5 m below the surface.

de-stratifies, due to slight warm up and subsequent wind-induced mixing. Hence, the estimated mixed-layer depth displays a high degree of short-term variability until mid-May (1994) or early April (1995), after which the stratification has a more permanent character.

The temporal-spatial evolution of the turbulent viscosity or diffusivity coefficient is detailed in Fig. 4b, with wind speed forcings plotted above (Fig. 4a). K_z attained minimal values of

$3 \times 10^{-5}\,m^2\,s^{-1}$ in the thermocline, $1 \times 10^{-4}\,m^2\,s^{-1}$ at 5 m above the bottom, $3 \times 10^{-5}\,m^2\,s^{-1}$ at 5 m below the air–sea interface. These values are significantly higher than the molecular kinematic viscosity of $1 \times 10^{-6}\,m^2\,s^{-1}$ and mainly result by imposing a minimal value below which the turbulent kinetic energy cannot drop ($1 \times 10^{-6}\,m^2\,s^{-2}$).

Due to the (almost) linear relationship between the square of the wind speed and turbulent kinetic energy at the air–sea interface (Table 1) and the linearity between the root of TKE and the eddy diffusivity, a strong linear relationship exists between surficial K_z values (5 m below the surface in the model) and wind speed ($r = 0.95$, $N = 730$, Fig. 4c). The surficial vertical diffusivities exhibit the same degree of short-term variability as the imposed wind forcing. At higher wind speeds, the water column is more thoroughly and deeply mixed (See Figs. 4a and b for two examples of such wind-induced mixing events). Periods of strong mixing alternate with periods where the water column is more stable. Wind speed was much lower in spring 1995 when compared to spring 1994 (contrast wind data after day 800 with wind after day 435). Consequently, the model predicts that stratification was several weeks earlier in 1995 (Fig. 3e, Fig. 4b).

3.2. *Biogeochemistry*

Essentially, the parameter values from Tett (1998) and Smith and Tett (2000) are used for the pelagic part of the model, whereas in the sediment submodel, the values are as reported in Soetaert et al. (1996a). To reproduce the data better, some fine-tuning of a selected number of parameter values was necessary.

The timing and magnitude of the spring phytoplankton bloom, the chlorophyll and micro-zooplankton distributions are reproduced by adjusting the zooplankton grazing and mortality parameters. Best results are obtained if the grazing rate is high ($5\,d^{-1}$ at 20°C). Combined with the settings for the assimilation efficiency and respiration rate (Fasham et al., 1990), this amounts to a maximal net growth rate of $0.875\,d^{-1}$ or a doubling time of less than a day. Some additional fine-tuning of the rate of water-column nitrification is necessary to obtain levels of reduced inorganic nitrogen, consistent with measured concentrations. In practice, the nitrification rate has been set to a low value of $0.05\,d^{-1}$ at 20°C as compared with a rate of $20\,d^{-1}$ in the sediment (Soetaert et al., 1996a).

In order to provide enough organic matter to the sediment, 14% of all detritus production consists of fast sinking material, (sinking rate of $100\,m\,d^{-1}$). In that case, the two measures of SCOC available are best matched by the model (Duineveld et al., 1997).

Finally, the benthic profiles sampled on two occasions, are fitted by adjusting the sediment mixing intensity. This parameter has only a marginal effect on the sediment community oxygen consumption rate, but it has a large impact on the nitrate and ammonium profiles (Soetaert et al., 1996a, 1998).

After this fine-tuning of parameters, the simulated water-column nitrate field resembles the observations in mean concentration, surface concentration and position and shape of the nitracline (Fig. 5a). Less variability exists in the modelled deep nitrate concentrations as compared to the data but the simulated values lie well within the observed scatter. Also ammonium concentrations and profiles correspond reasonably to the data, although the deep concentration in the model may be slightly too low in winter (Fig. 5b; day 370).

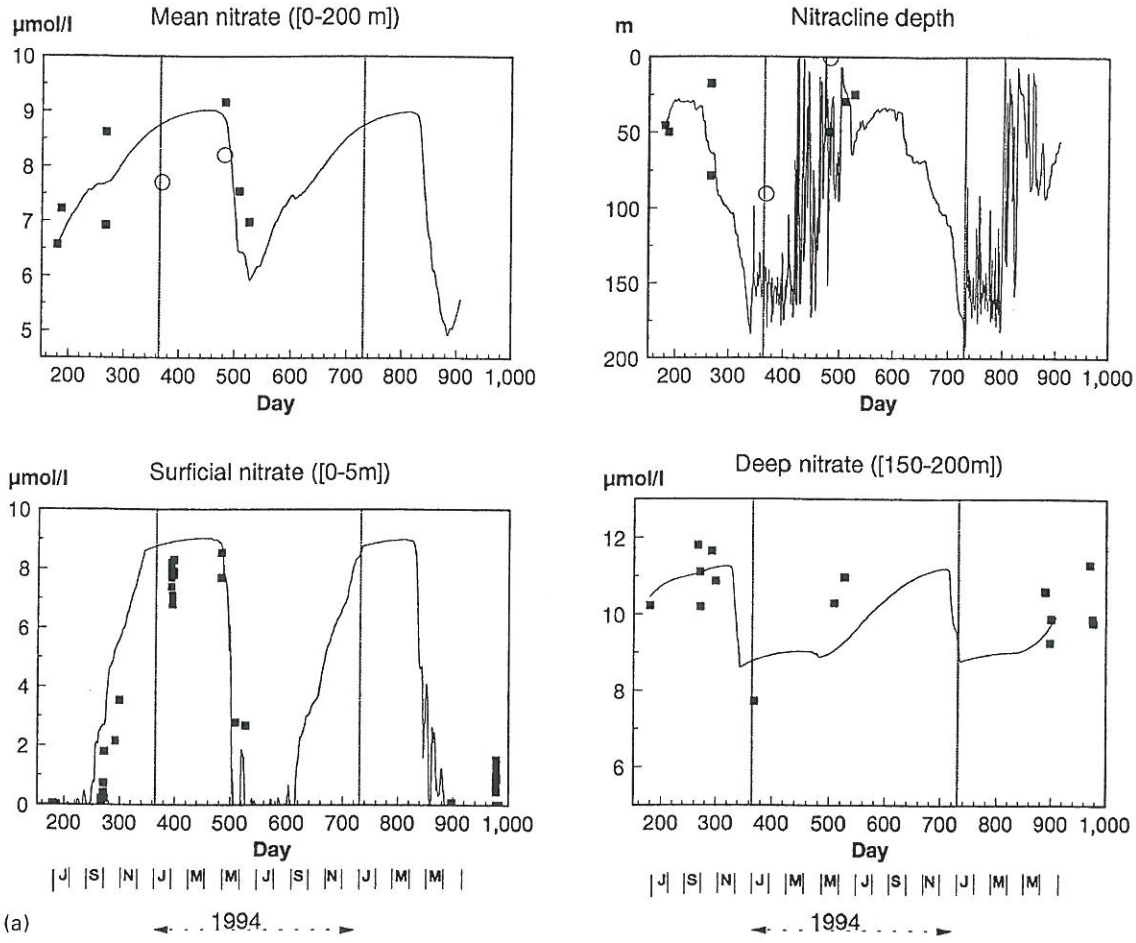

Fig. 5. a. Fit of modelled and observed nitrate concentrations ($\mu mol\,l^{-1}$, mean, surficial and deep concentration) and nitracline depth (m). Circles are data for which the two-layer model used to fit the data was not significantly better than the constant nitrate concentration model. (see material and methods). b. Fit of modelled and observed ammonium concentrations ($\mu mol\,l^{-1}$, mean, surficial and deep concentration) and depth of ammonium maximum (m). Solid squares are data for which the non-linear fitting of profiles by means of a shifted Gaussian was significantly the best; circles are data for which a constant concentration model was significantly best. c. Fit of modelled and observed oxygen concentrations ($\mu mol\,l^{-1}$, surficial and deep concentration).

Oxygen concentrations in the upper 5 m of the water column exhibit super-saturated concentrations year-round, in accordance with the data (Fig. 5c). Super-saturation in fall and winter is due to bubble injection, while in spring, super-saturation is of biotic origin. In spring 1994, the modelled oxygen concentration appears somewhat too high; also, the model tends to have too much oxygen in the deeper parts of the water column (Fig. 5c). In general, the order of magnitude of the simulated chlorophyll concentration and the timing of the bloom is similar to the observations. The mean chlorophyll concentration in the upper 100 m of the water column is, however, too high in the simulation (Fig. 6a). Additionally, the position of the chlorophyll maximum in the water column agrees reasonably well with the available data (Fig. 6a). In the model, the chlorophyll maximum is the result of both the increase in phytoplankton biomass and

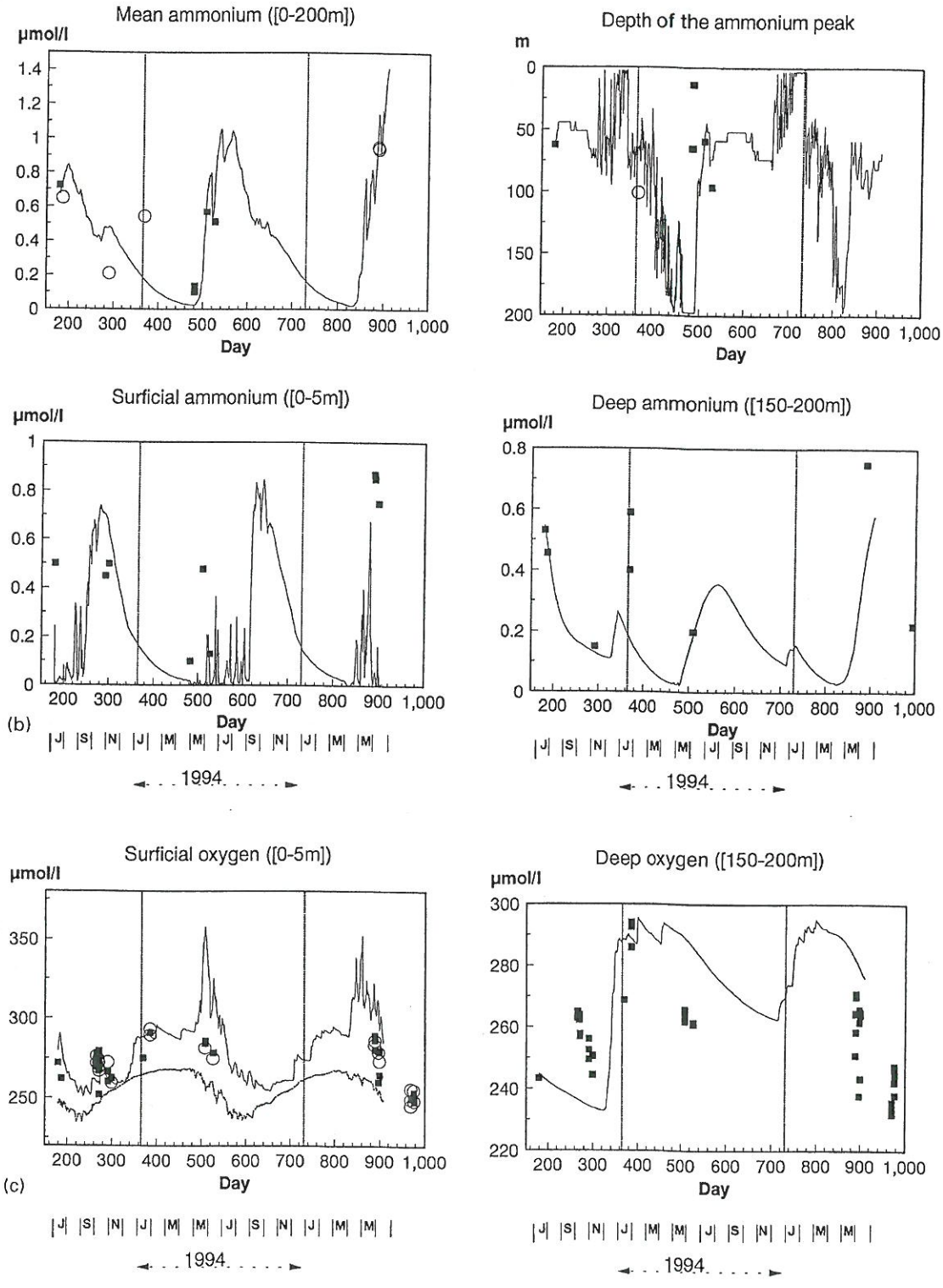

Fig. 5. (*continued*)

the increase in the chlorophyll/carbon ratio for algae residing at low light levels. In general, the few observations on microzooplankton biomass are well represented by the simulation (Fig. 6c). Modelled and measured oxygen fluxes at the sediment–water interface are comparable (Fig. 7a). In addition, the diagenetic submodel is able to reasonably reproduce the shape of the various profiles obtained in October 1993 and May 1994 (Fig. 7b).

The net euphotic zone primary production estimate for the year 1994 is $203\,gC\,m^{-2}\,a^{-1}$ (Fig. 6b). This value is somewhat larger than the estimate of $163\,gC\,m^{-2}\,a^{-1}$, based on a compilation of data from various years for the region (Joint et al., 2001).

As a check on the nitrogen budget, we a posteriori compared modelled with ^{15}N-uptake and satellite-based values of the "*f*-ratio" (Joint et al., 2001), i.e. the euphotic-zone nitrate uptake rate as a fraction of total (nitrate + ammonium) N-uptake (Fig. 6b). We discarded those few values where ammonium assimilation was negative (indicating net excretion rather than net assimilation). Model prediction agrees well with observations (Fig. 6b). The contribution of nitrate to total N assimilation exhibits a clear seasonal cycle as well as short-term variability.

4. Discussion

4.1. Description of modelled system dynamics in the year 1994

Temporal-spatial patterns of the temperature, chlorophyll, nitrate and ammonium fields in the water column and of oxygen, nitrate and ammonium in the sediment, for the year 1994 are provided in Fig. 8. Strong winds and low heat input keep the water column well mixed until about the end of April, when stratification begins. As the water column becomes more stable, the mixing depth shoals and the mean light experienced by the algae increases. The interplay of this, together with the intensity of zooplankton grazing allows the development of the spring bloom. Being mainly sustained by nitrate supplied by winter mixing, the primary production is new production, as indicated by a high *f*-ratio (Fig. 6b). After depletion of nitrate in the euphotic zone, the standing stock of phytoplankton is determined by the in situ regeneration of inorganic nitrogen as ammonium (characterised by a low *f*-ratio; Fig. 6b) and the extent to which nutrients are physically mixed upward into the euphotic zone. Singular storms provoke deep mixing, replenishing nutrients in the upper layer of the water column and fuelling new primary production. This is discernible in the model as short-term increases of the nitrate and ammonium concentration in the surface layer (Figs. 5a, b and 8a) and as short-term increases in the relative importance of the uptake of nitrate (Fig. 6b). These wind-driven events are also possibly recognisable in the data. For instance, at the onset of the phytoplankton bloom, a similar surface nitrate concentration, intermediate to winter and summer values, was measured at about 2–3 weeks interval (Fig. 6a; day 508, 526). Apparently, a preceding windy period, causing nutrient entrainment, markedly enhanced the concentration of nitrate in the upper layer during the second measurement (see also Fig 4).

Part of the phytoplankton sinks below the mixed layer, where its mineralisation generates a pronounced ammonium peak, tapering off towards the bottom (Fig. 8a). As a result, the mean ammonium concentration rises well above $1\,\mu mol\,l^{-1}$ (Fig. 5b). Subsequent oxidation of this

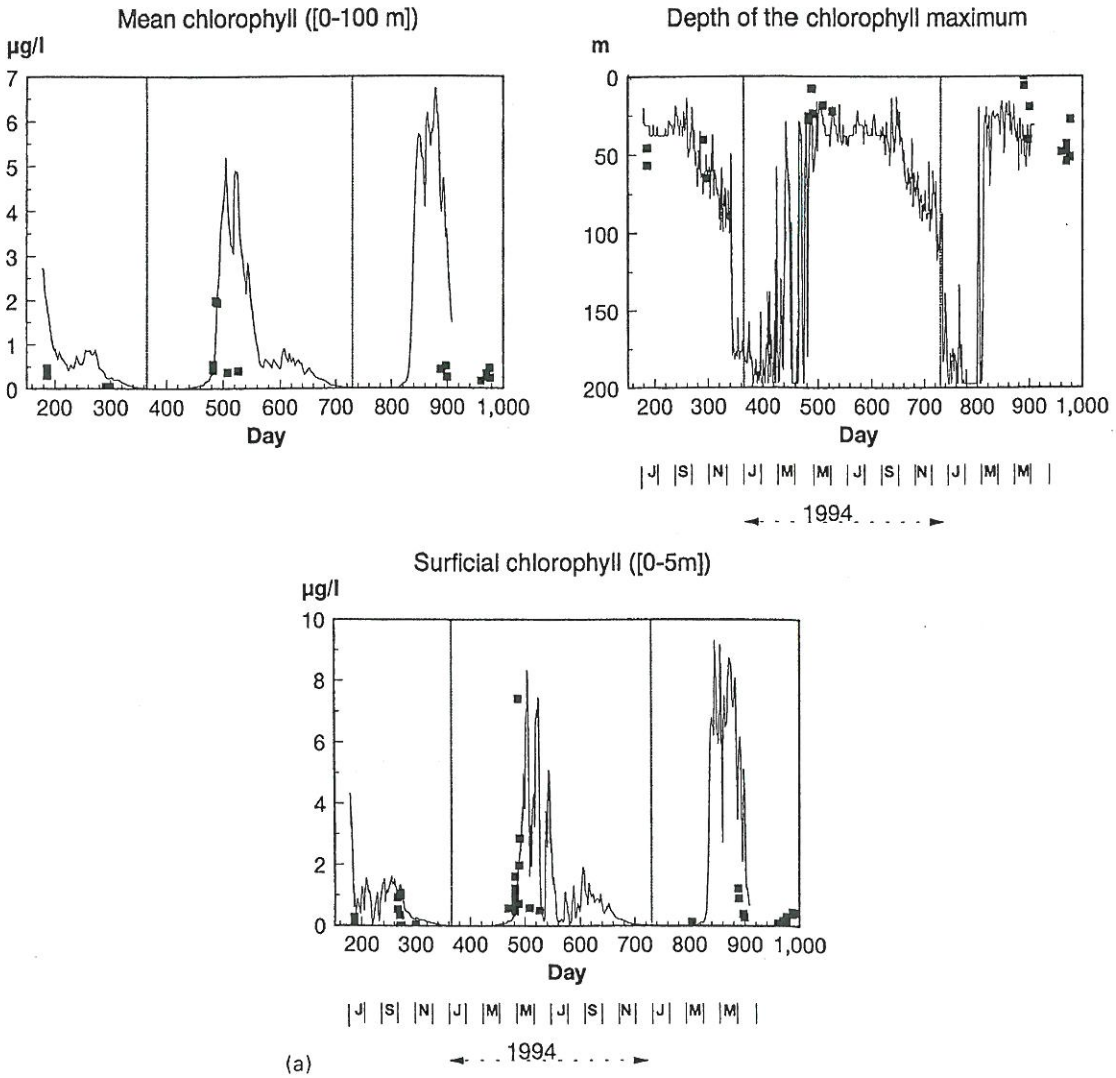

Fig. 6. a. Fit of modelled and observed chlorophyll concentrations ($\mu g\,l^{-1}$, mean, surficial) and the position of the chlorophyll maximum (m). b. Fit of modelled and measured euphotic zone primary production (left, mmol-C $m^{-2}\,d^{-1}$) and the euphotic-zone nitrate uptake rate as a fraction of total (nitrate + ammonium) N-uptake (right, f-ratio) based on satellite observations and ^{15}N techniques. c. Fit of modelled and observed microzooplankton concentration in the upper 10 m of the water column (μmol-C l^{-1}).

ammonium replenishes the winter stocks of nitrate, while ammonium concentrations drop to very low values by the end of winter (Figs. 5a, b and 8a).

The simulated sediment properties display far less short-term fluctuations than the pelagic system (Figs. 7 and 8b). Only the nitrate profiles reflect, to a certain degree, the short-term variability in organic matter deposition, whereas the other constituents change more smoothly in time. Nevertheless, there is an important seasonality in the modelled concentrations and the sediment–water fluxes. After deposition of the spring bloom, sediment ammonium concentrations rapidly increase and migrate upward, whereas nitrate and oxygen are quickly consumed. Hence,

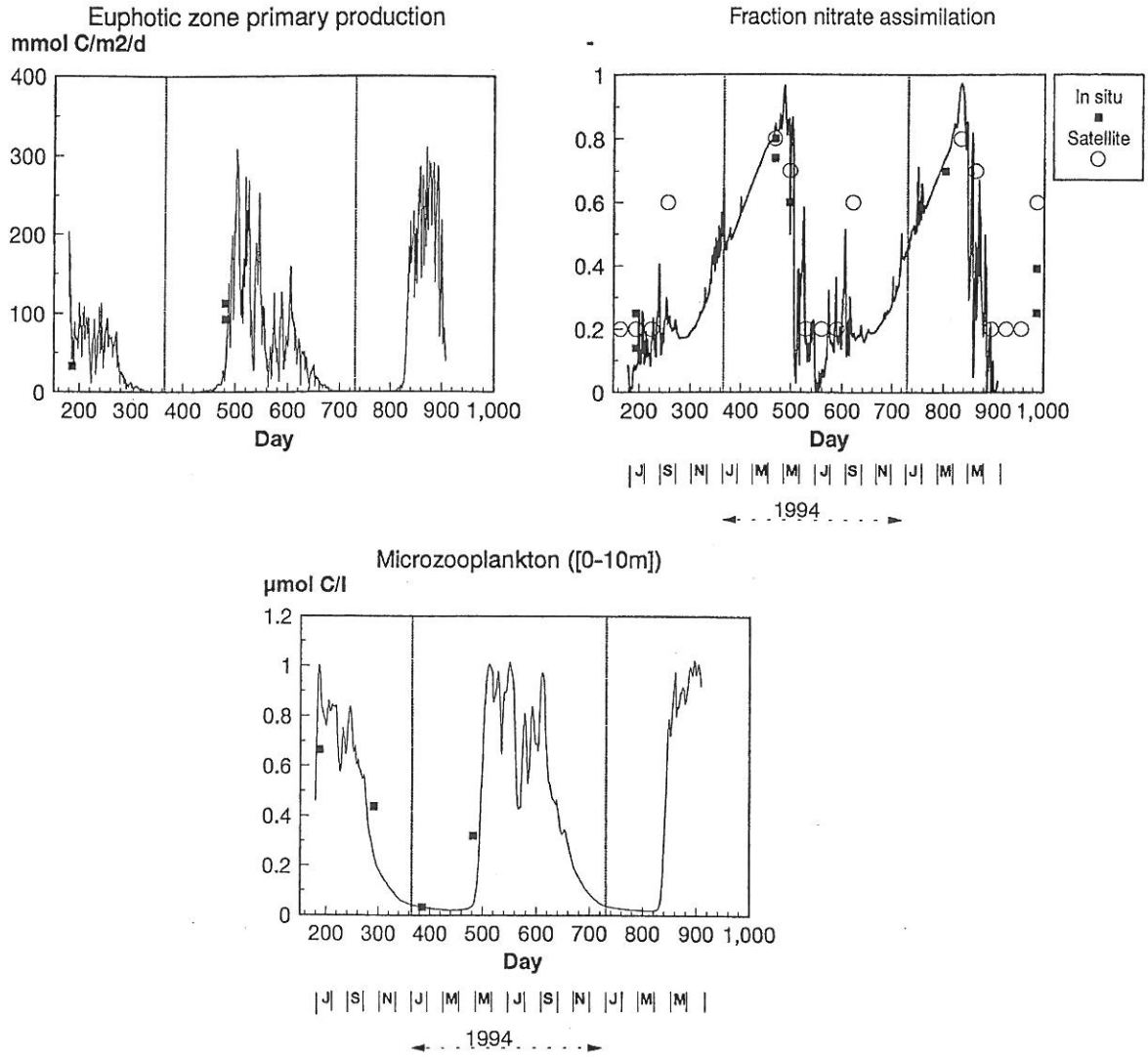

Fig. 6. (*continued*)

the oxygen penetration depth decreases from about 2.5 cm to less than 1 cm in about 10 days time. Over the year, oxygen fluxes vary from 1.1 to 9.5 mmol $m^{-2} d^{-1}$, i.e., almost a 10-fold difference between minimal and maximal rates (Fig. 7a).

While the evidence for such a large benthic variability may not be overwhelming (considering the fact that sampling occurred on only two occasions and yielded very similar results), it is reassuring that the model was able to capture the main features in the sediment profiles. Also, some of the subtleties in the ammonium profiles are, to a certain extent, reproduced by the model, with a sharper gradient in fall 1993 (retreating ammonium profile; Fig. 7b) when compared to those in spring 1994 when ammonium concentrations have a gentler slope (i.e., upward migration of ammonium; Fig. 7c).

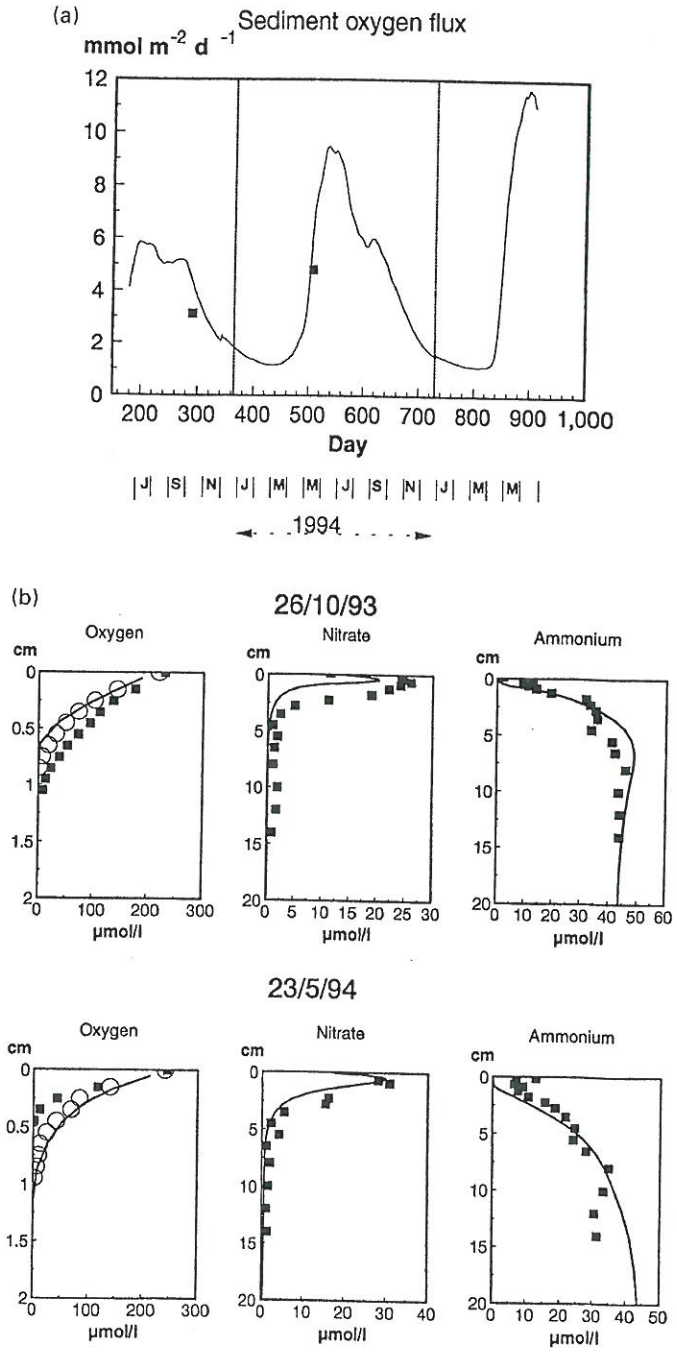

Fig. 7. a. Fit of modelled and observed sediment community oxygen consumption rates ($mmol\,m^{-2}d^{-1}$). b. Fit of modelled and observed sedimentary oxygen, nitrate and ammonium profiles obtained at day 291 (26/10/93) and at day 508 (23/05/94).

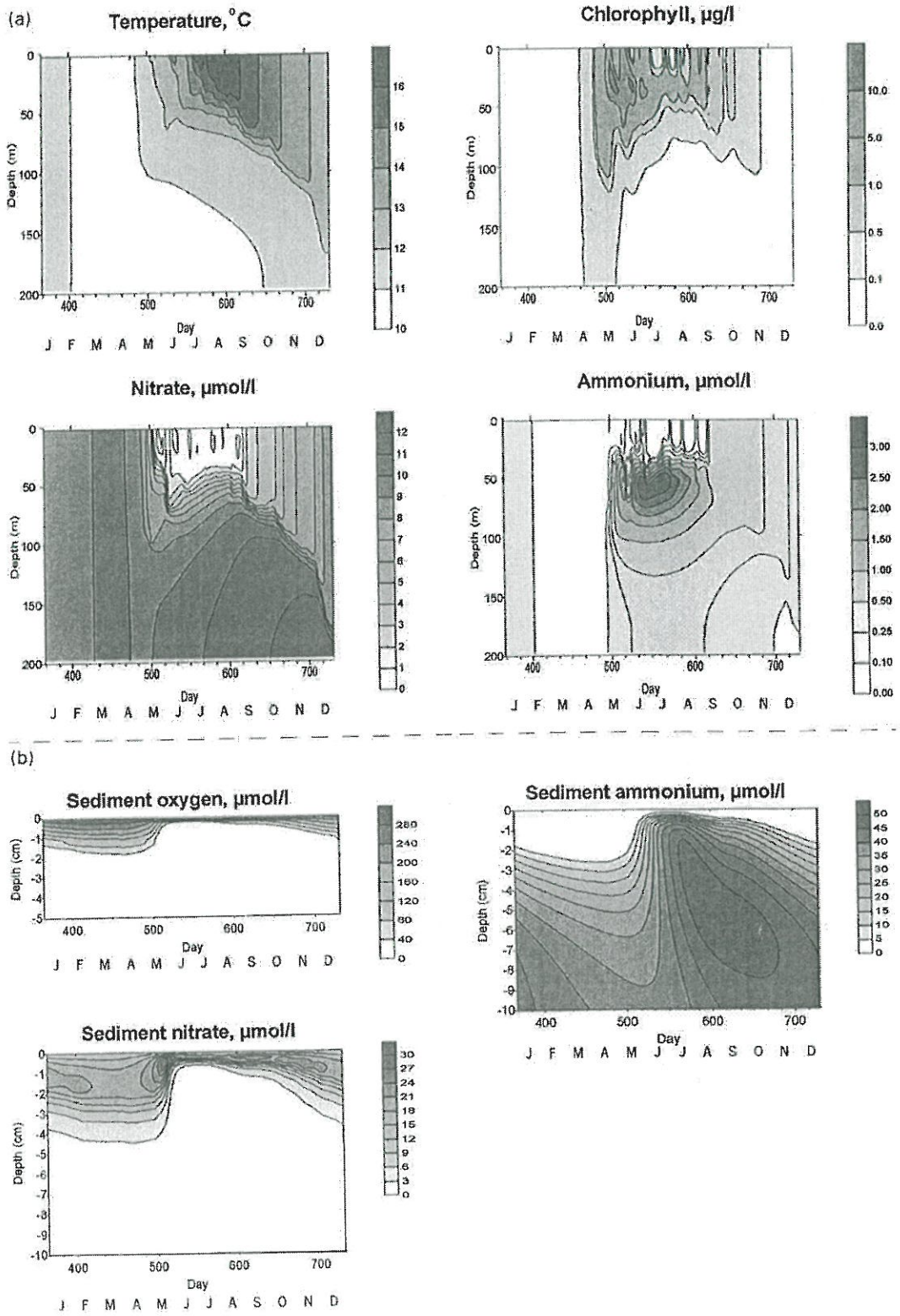

Fig. 8. a. Spatio-temporal plot of the modelled fields of temperature, chlorophyll, nitrate and ammonium in the water column for the year 1994. b. Spatio-temporal plot of the oxygen, ammonium and nitrate concentrations in the sediment for the year 1994.

The net euphotic zone primary production in 1994 was 203 $gC\,m^{-2}\,a^{-1}$, which is somewhat higher than the estimate of 163 $gC\,m^{-2}\,a^{-1}$ for the area, based on a compilation of data from various years (Joint et al., 2001). About 15 $gC\,m^{-2}\,a^{-1}$, i.e. about 7% of euphotic-zone net production, is respired by the benthic community in the model.

4.2. The 1994 nitrogen budget

The annual N-budget within the euphotic zone, the aphotic zone and the sediment predicted by the model for the year 1994 is illustrated in Fig. 9. (Note that the euphotic zone is defined as the depth where the PAR is 1% of the surface radiation). Due to the small differences in standing stock of some constituents at the beginning and end of the integration period, the budget appears slightly unbalanced, but total nitrogen is conserved in the model.

In 1994, an amount of 2.6 mol-N m^{-2} was converted from dissolved into particulate form and vice versa. Compared with the total nitrogen load (excluding the refractory DON), this leads to a mean turnover time of water column nitrogen of less than a year. Below the euphotic zone, net carbon intake stops, but the algae continue to assimilate nitrogen (luxury consumption of DIN) until the N:C ratio attains a maximal value. In the model about 23% of total nitrogen assimilation thus occurs below the euphotic zone (Fig. 9b). Photic and dark N-assimilation involve mainly ammonium (60%, 1536 mmol-N $m^{-2}\,a^{-1}$); the remaining 40% (1016 mmol-N $m^{-2}\,a^{-1}$) is assimilated in the form of nitrate (Fig. 9a). As respiration releases inorganic nitrogen as ammonium, an amount equivalent to nitrate assimilation is nitrified per year (1013 mmol-N $m^{-2}\,a^{-1}$; Fig. 9a). In the model, the main site of nitrification is in the water column below the euphotic zone (66%), but a non-negligible part (17%) occurs in the euphotic zone. The remaining nitrate regeneration (17%) is due to sedimentary nitrification (Fig. 9b). The sources of nitrate in the euphotic zone are in situ nitrification (21%), mixing from below the euphotic zone (78%) and lateral sources (1%, necessary to compensate for the loss due to denitrification, see below, Fig. 9a). In the water column below the euphotic zone, 80% of the nitrate is derived from in situ nitrification, 12% from the sediments, 8% from lateral sources (Fig. 9a). Ammonium regeneration below the euphotic zone is mainly a water-column process (99%); only 1% is derived from the sediment. Euphotic zone ammonium mainly originates from in situ mineralisation, whereas only 19% is derived from mixing below the euphotic zone.

The amount of organic nitrogen sinking out of the euphotic zone is 873 mmol-N $m^{-2}\,a^{-1}$, i.e., about 44% of total euphotic zone N assimilation. About 187 mmol-N $m^{-2}\,a^{-1}$ are incorporated in the sediment (Fig. 9a), where the derived ammonium is nearly completly oxidised (95%). Forty-four percent of the nitrate thus formed is denitrified in the sediment; the other part is returned to the water column. Due to the efficiency with which ammonium is re-oxidised, the impact of the sediment on the total system nitrification is much larger (17%) than on total system respiration (7%) (Fig. 9b).

Several conclusions can be drawn from this budget. First of all, water-column nitrification is much more important than sedimentary nitrification, the latter accounting for a meagre 17%. This seems to be in contradiction with several orders of magnitude higher nitrification rates (expressed as d^{-1}) in the sediment, but here the process is restricted to the oxygenated upper centimetre, whereas it may occur in the entire 200 m of the upper water column. We arrived at an areal estimate of water-column nitrification of 2.3 mmol-N $m^{-2}\,d^{-1}$, which compares favourably

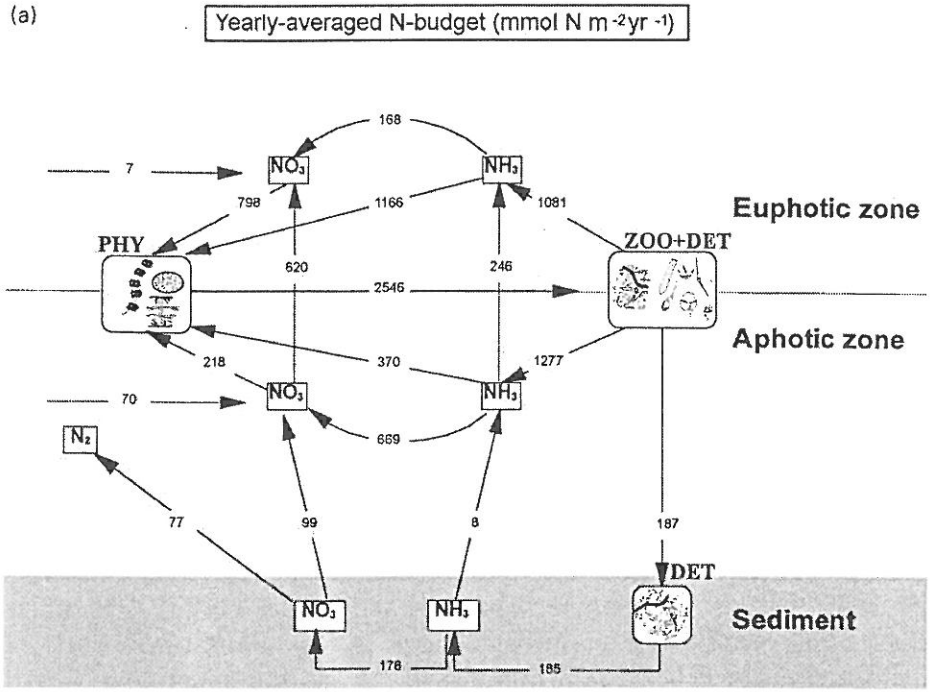

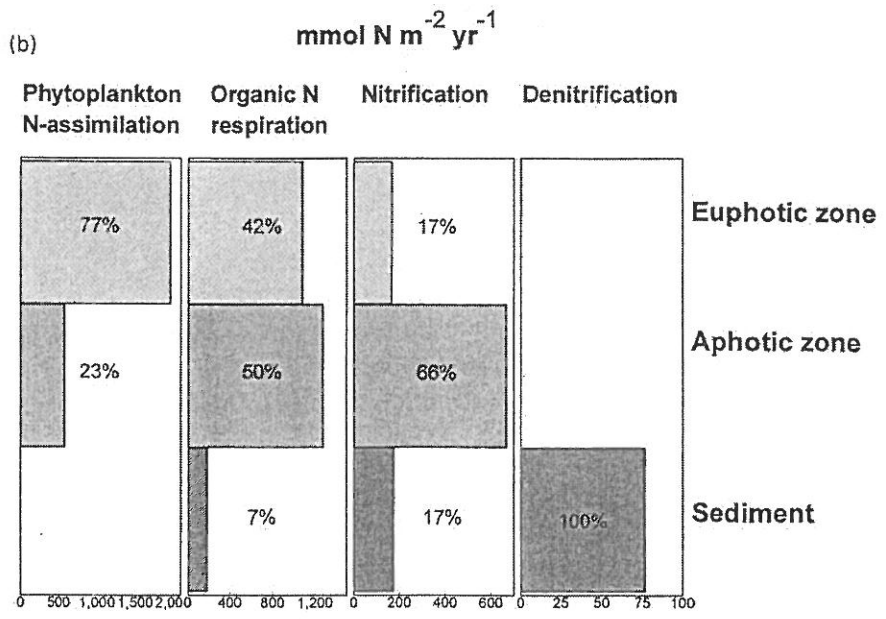

Fig. 9. Yearly-averaged nitrogen budget (1994) of the euphotic zone (defined as the depth where 1% of surficial PAR is retained), the water column below the euphotic zone (aphotic), and the sediment. All fluxes are in mmol-N $m^{-2} a^{-1}$. For comparison, the average total load of pelagic nitrogen was 1840 mmol m^{-2}, benthic nitrogen (upper m) amounts on average to 265 mmol m^{-2}. (a) the N-fluxes to the phytoplankton (left), the pelagic detritus + microzooplankton (right) and the sediment compartment; (b) the relative contribution of the main processes in the three zones.

with measured nitrification rates of 0.5–1.6 mmol-N $m^{-2} d^{-1}$ from the lower euphotic zone of a North Pacific deep-sea station (Dore and Karl, 1996). The oxidation rate of 0.05 d^{-1} at 20°C, obtained after fine-tuning, is the same as the rate used in a model of the Black Sea by Oguz et al. (1996). While most simulation models apparently can do without water-column nitrification, in general these models have a lower boundary forcing the ammonium to low and nitrate to high values. A notable exception is the model of Kühn and Radach (1997), for the spring bloom in the northern North Sea; however, their simulation did not include the second part of the year, when nitrification may be important. Our model explicitly includes sedimentary nitrification, the magnitude of which is constrained by fitting the sediment profiles from the area. Without the extra water-column nitrification, model-generated ammonium profiles did not exhibit a marked peak, but instead behaved more like nitrate.

The quantity of nitrogen lost through sedimentary denitrification is remarkably low (77 mmol-N $m^{-2} a^{-1}$), amounting to somewhat less than 3% of net nitrogen assimilation. Compared to total pelagic nitrogen load, 4% is denitrified per year and must be replenished from other sources. In the model, this nitrogen loss is input via lateral transport of nitrate. In terms of total nitrogen fluxes, this lateral input is therefore of minor importance (but note that it may be an underestimation). In addition, the Goban Spur shelf-break sediments cannot be considered an important sink for nitrogen, in contrast to estimates from many other shelf areas (Christensen et al., 1987; Middelburg et al., 1997).

4.3. *New versus regenerated euphotic zone production*

Phytoplankton nitrogen assimilation is commonly divided into 'new' production, resulting from external supply to the euphotic zone and 'regenerated' production, resulting from nitrogen recycled within the euphotic zone. An operational definition considers new production to be equivalent to nitrate uptake, while ammonium assimilation is equated to regenerated production. This working definition assumes that recycling in the euphotic zone results in the release of ammonium only, that recycling is the sole source of euphotic-zone ammonium, and that in situ production of nitrate in the euphotic zone is negligible. However, euphotic zone nitrification can be coincident with nitrate assimilation (Ward et al., 1989, Bianchi et al., 1997), and this, added to measurement uncertainties (Elskens et al., 1995), may seriously affect the applicability of the operational definition of new and regenerated productions. We can examine in our model, how the violations of the underlying assumptions affect the estimated amount of new production. Nitrate accounts for 41% of the yearly averaged nitrogen assimilation in the euphotic zone (798 mmol-N $m^{-2} a^{-1}$), leading to a nitrate/total N assimilation ratio of 0.41. However, nitrate assimilation is not equivalent to total new production for two reasons. Firstly, 21% of the euphotic-zone nitrate uptake is derived from in situ nitrification; hence, uptake of this nitrate is, in reality, a regenerated production. Secondly, not all of the assimilated ammonium in the euphotic zone is derived from in situ respiration and mineralisation; some 21% (246 mmol-N $m^{-2} a^{-1}$) is mixed into the euphotic zone and, hence, reflects further a new source of nitrogen. Considering all the sources of inorganic nitrogen in the euphotic zone led to a 'new' production of about 866 mmol-N $m^{-2} a^{-1}$ (or a new/total production of 0.44). As the in situ nitrification is nearly balanced by the import of ammonium into the euphotic zone, the amount of new production is

not far from the amount estimated from nitrate assimilation. Due to that the calculated ratio of nitrate/total N assimilation is very near to the ratio new/total N production.

4.4. *Weather versus climatological forcing*

Recent modelling papers have addressed the impact of distant forcing (McGillicuddy et al., 1995; Smith et al., 1996) and of in situ weather conditions on the vertical structure of the water column (Ridderinkhof, 1992) and ecosystem dynamics (Sharples and Tett, 1994; Bissett et al., 1994; Radach and Moll, 1993; Tusseau et al., 1997). These have shown that atmospheric variability may affect the generation of the deep chlorophyll maximum (Sharples and Tett, 1994), may increase the system productivity (Bissett et al., 1994), or may impact the ratio of new versus regenerated productivity (Jenkins and Goldman, 1985).

By means of our 1-D model, we can demonstrate the impact of short-term variability in weather conditions on biological processes in the Goban Spur area and how this variability propagates through the water column. To do so, we compare our original model results with a test model solution based on climatological (i.e., seasonally smoothed) forcing. The integrated momentum added to the sea by the forcing is reduced by the smoothing mechanism. We ran the model for several years until a recurrent steady-state was established and the heat budget closed. For most atmospheric variables, the forcing consisted of a sine function, the parameters of which were derived from the original forcing data. For the atmospheric pressure, a constant value was used. The impact on the pelagic system was dramatic (Fig. 10). Yearly averaged, the upper 5 m of the water column was about 5% warmer, while the deep water layer was about 3% cooler; mean water-column temperature was 2.5% lower in the climatological run. In addition, the stratification started somewhat earlier. Using seasonally smoothed forcing, the euphotic-zone primary production started earlier than 1994 when using real weather data, but did not last long. It attained about 145 $gC\,m^{-2}\,a^{-1}$, compared to approximately 203 $gC\,m^{-2}\,a^{-1}$ when using real-

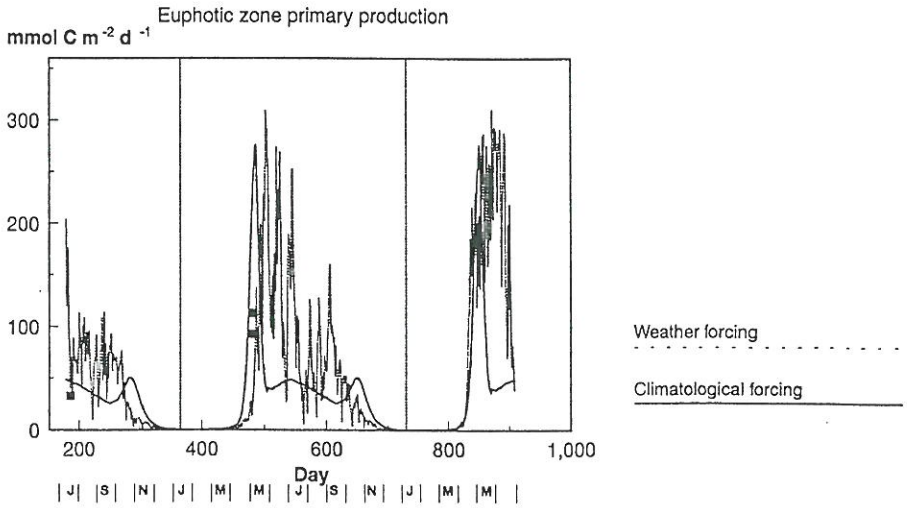

Fig. 10. Comparison of euphotic zone production based on a model run with weather forcing (3-hourly resolution, dashed line) and atmospheric forcing (smooth sinus function or constant forcing, solid line).

weather forcing. Euphotic zone nitrogen assimilation decreased by about 20%. Due to the absence of episodic nutrient input to the euphotic zone, the euphotic-zone nitrogen assimilation depends relatively more on regenerated forms of nitrogen; 38% of assimilated nitrogen is derived from mixing below the nutricline. This amounts to a new/total euphotic-zone production ratio of 0.38, in contrast to 0.44 under more realistic weather forcing (see above).

The impact of intermittent, wind-driven mixing events is mainly restricted to the euphotic zone, where nutrients may be injected due to erosion of the nutricline, introducing variability in euphotic zone production and concentrations (Fig. 8a). Deep-water concentrations vary much more smoothly (Figs. 6, 7 and 8a).

The large variability in euphotic zone net production is reflected in the carbon deposition on the sediment (not shown) and also to a certain extent in the resulting nitrate profiles and fluxes. Neither the ammonium and oxygen profiles nor the resulting fluxes at the sediment–water interface showed high-frequency oscillations of comparable magnitude (Fig. 8b).

4.5. *Microzooplankton versus mesozooplankton*

Essential to the performance of the model is the parameterization of herbivore consumption to a value typical for microzooplankton-like grazing. Only when grazing rates are sufficiently high (attaining a maximal rate of $5\,d^{-1}$ at 20°C) is it possible to obtain acceptable low phytoplankton levels in summer, while still retaining a sufficiently high primary production. The value of $5\,d^{-1}$ is about the mean grazing rate ascribed to ciliates (Hansen et al., 1997), the dominant microzooplankton group in the OMEX area (Edwards et al., 1995). When imposing grazing rates typical for mesozooplankton consumption (maximal grazing rate $1\,d^{-1}$ at 20°C; Henderson and Steele, 1995), chlorophyll concentrations remain too high after the spring bloom, while exhibiting a peak too deep in the water column (results not shown). Similarly, Carlotti and Radach (1996) were unable to limit the extent of the spring bloom with grazing by the large copepod Calanus finmarchicus, and these results are in line with the growing body of evidence that microzooplankton are the main herbivores in the marine environment. During the North Atlantic Bloom experiment (47°N 20°W), mesozooplankton grazing was small (Dam et al., 1993), whereas the microzooplankton consumed significant amounts of phytoplankton (Burkill et al., 1993) during the spring period. According to the latter authors, the microzooplankton were able to consume 100–800% of their biomass per day (compared to a maximal grazing rate of $5\,d^{-1}$ in our model).

Nevertheless, we may have overstressed the importance of microzooplankton grazing. In our model about 80% of euphotic zone production is channelled through the grazers, whereas Joint et al. (2001) arrived at 50–60% only, of which the majority is attributed to mesozooplankton. Possibly, we may have aliased (micro) zooplankton grazing with other processes, working on similarly short time scales (say about 1 day or less). Certainly, explicit accounts of aggregation/disaggregation processes and their impact on physical sinking are missing from our model. Possibly our microzooplankton grazing may, in part, reflect this process. Indicative in this respect is the fact that, in order to fuel sediment metabolism, about 14% of detritus production must sink with a settling velocity of $100\,m\,d^{-1}$. This could either reflect meso-zooplankton grazing or aggregate formation.

5. Conclusion

We have successfully coupled a physical–biogeochemical pelagic model with a dynamic model of early diagenetic processes and applied this to the shelf break environment at the Goban Spur. Our shelf-break model differs from other coupled dynamic models mainly in the explicit inclusion of a dynamic description of diagenetic processes. The benthic profiles may be used as a constraint on the water column dynamics (see also Herman et al., 2001), whereas the pelagic model provides constraints (deposition fluxes, bottom water conditions) on the benthic model.

By using high-frequency atmospheric forcing, the effect of in situ physical variability on biogeochemical processes is highlighted. Short-term variability in system response is mainly restricted to the euphotic zone, whereas deep concentrations and sediment properties are less affected. Due to the inclusion of short-term mixing events, the euphotic zone carbon production increases about 40% and the nitrogen assimilation about 20%, mainly due to new production.

We have restricted our modelling exercise to a fine-tuning of model parameters, which we believed to be least well known, so that we reproduced, as faithfully as possible, a large set of measurements performed within the OMEX project. By doing so, we were able to derive a tentative nitrogen budget, demonstrating the impact of the euphotic zone, the water column below the euphotic zone, as well as the sediments, in total nitrogen assimilation, mineralisation and nitrification.

Acknowledgements

The authors are greatly indebted to all those persons who collected the data on which our model so crucially depended. The BODC provided a very efficient facility through which these data sets could be accessed. Special thanks to Bernard Boudreau, Günther Radach and an anonymous referee for the many useful suggestions. Weather forcings were obtained from the UK Meteorological office. This work was performed in the framework of the EU-MAST II & III supported Ocean Margin EXchange (OMEX) project (MAS2-CT93-0069, MAS3-CT96-0056).

References

Berner, R.A., 1980. Early Diagenesis—a Theoretical Approach. Princeton University Press, Princeton, New York, 241pp.

Bianchi, M., Feliatra, F., Tréguer, P., Vincendeau, M.-A., Morvan, J., 1997. Nitrification rates, ammonium and nitrate distribution in upper layers of the water column and in sediments of the Indian sector of the Southern Ocean. Deep-Sea Research II 44 (5), 1017–1032.

Bissett, M.P., Meyers, M.B., Walsh, J.J., Müller-Karger, F.E., 1994. The effects of temporal variability of mixed layer depth on primary productivity around Bermuda. Journal of Geophysical Research 99 (C4), 7539–7553.

Blanc, T.V., 1985. Variation of bulk-derived surface flux, stability and roughness results due to the use of different transfer coefficient schemes. Journal of Physical Oceanography 15, 650–669.

Blanke, B., Delecluse, P., 1993. Variability of the tropical Atlantic ocean simulated by a general circulation model with two different mixed-layer physics. Journal of Physical Oceanography 23, 1363–1388.

Blumberg, A., Mellor, G., 1987. A description of a three-dimensional coastal ocean circulation model. Coastal and estuarine science 4, 1–16.

Boudreau, B.P., 1996. Diagenetic Models and their Implementation. Modelling Transport and Reactions in Aquatic Sediments. Springer, Berlin, 414 pp.

Bougeault, P., Lacarrère, P., 1989. Parameterization of orography-induced turbulence in a mesobeta-scale model. Monthly Weather Review 117, 1872–1890.

Burkill, P.H., Edwards, E.S., John, A.W.G., Sleigh, M.A., 1993. Microzooplankton and their herbivorous activity in the northeastern Atlantic Ocean. Deep-Sea Research part II 40 (1/2), 479–494.

Carlotti, F., Radach, G., 1996. Seasonal dynamics of phytoplankton and Calanus finmarchicus in the North Sea as revealed by a coupled one-dimensional model. Limnology and Oceanography 41 (3), 522–539.

Christensen, J.P., Murray, J.W., Devol, A.H., Codispoti, L.A., 1987. Denitrification in continental shelf sediments has major impact on the oceanic nitrogen budget. Global Biogeochemical Cycles 1, 97–116.

Clarke, T., 1986. A two layer model of the seasonal thermocline and its application to the north west European continental shelf seas. Report U86-2, University of Wales, Bangor, Unit for Coastal and Estuarine Studies,

Dam, H.G., Miller, C.A., Jonasdottir, S.H., 1993. The trophic role of mesozooplankton at 47°N, 20°W during the north Atlantic bloom experiment. Deep-Sea Research part II. 40 (1/2), 197–212.

Dore, J.E., Karl, D.M., 1996. Nitrification in the euphotic zone as a source for nitrite, nitrate, and nitrous oxide at Station ALOHA. Limnology and Oceanography 41 (8), 1619–1628.

Duinveld, G.C.A., Lavaleye, M.S.S., Berghuis, E.M., De Wilde, P.A.W.J., Van Der Weele, J., Kok, A., Batten, S.D., De Leeuw, J.W., 1997. Patterns of benthic fauna and benthic respiration on the Celtic continental margin in relation to the distribution of phytodetritus. Internationale Revue der gesamten Hydrobiologie 82, 395–424.

Edwards, E.S., Burkill, P.H., Stelfox, C.E., 1995. Microzooplankton abundance and biomass in the Goban Spur, Celtic Sea. Ocean Margin Exchange, Second Annual Report, pp. D83–D90.

Edinger, J.E., Duttweiler, D.W., Geyer, J.C., 1968. The response of water temperatures to meteorological conditions. Water Resources Research 4, 1137–1145.

Elskens, M., Goeyens, L., Dehairs, F., 1995. Bioreactive elements in the suspended matter. OMEX Annual Report, pp. D31–D40.

Fasham, M.J.R., Ducklow, H.W., McKelvie, S.M., 1990. A nitrogen-based model of plankton dynamics in the oceanic mixed layer. Journal of Marine Research 48, 591–639.

Gaspar, P., Grégoris, Y., Lefevre, J-M., 1990. A simple eddy kinetic energy model for simulations of the oceanic vertical mixing: tests at Station Papa and long-term upper ocean study site. Journal of Geophysical Research 95 (C9), 16179–16193.

Hadfield, M.G., Sharples, J., 1996. Modelling mixed layer depth and plankton biomass off the west coast of South Island, New Zealand. Journal of Marine Systems 8, 1–29.

Hansen, P.J., Bjørnsen, P.K., Hansen, B.W., 1997. Zooplankton grazing and growth: scaling within the 2-2000 μm body size range. Limnology and Oceanography 42 (4), 687–704.

Henderson, E.W., Steele, J.H., 1995. Comparing models and observations of shelf plankton. Journal of Plankton Research 17 (8), 1679–1692.

Herbland, A., Voituriez, B., 1978. Hydrological structure analysis for estimating the primary production in the tropical Atlantic ocean. Journal of Marine Research 37 (1), 87–101.

Herman, P.M.J., Soetaert, K., Middelburg, J.J., Heip, C., Lohse, L., Epping, E., Helder, W., Antia, A.N., Peinert, R., 2001. The seafloor as the ultimate sediment trap—using sediment properties to constrain benthic–pelagic exchange processes at the Goban Spur. Deep-Sea Research II 48, 3245–3264.

Jenkins, W.J., Goldman, J.C., 1985. Seasonal oxygen cycling and primary production in the Sargasso Sea. Journal of Marine Research 43, 465–491.

Joint, I., Rees, A., 1995. Primary and new production. Ocean Margin Exchange, Second Annual Report, pp. D73–D82.

Joint, I., Rees, A., Pomroy, A., 1994. Primary and new production. In Ocean Margin Exchange, First Annual Report, pp. D75–D82.

Joint, I., Wollast, R., Chou, L., Batten, S., Elskens, M., Edwards, E., Hirst, A., Burkill, P., Groom, S., Gibb, S., Miller, A., Hydes, D., Dehairs, F., Antia, A., Barlow, R., Rees, A., Pomroy, A., Brockmann, U., Cummings, D., Lampitt, R., Loijens, M., Mantoura, F., Miller, P., Raabe, T., Alvarez-Salgado, X., Stelfox, C., Woolfenden, J., 2001. Pelagic production at the Celtic Sea shelf break. Deep-Sea Research II 48, 3049–3081.

Kiefer, D.A., Kremer, J.N., 1981. Origins of vertical patterns of phytoplankton and nutrients in the temperate, open ocean: a stratigraphic hypothesis. Deep-Sea Research 28 A (10), 1087–1105.

Kühn, W., Radach, G., 1997. A one-dimensional physical–biological model study of the pelagic nitrogen cycling during the spring bloom in the northern North sea (FLEX '76). Journal of Marine Research 55, 687–734.

Kurihara, Y., 1965. On the use of implicit and iterative methods for the time integration of the wave equation. Monthly Weather Review 93 (1), 33–46.

Laws, E.A., Wong, D.C.L., 1978. Studies on carbon and nitrogen metabolism by three marine phytoplankton species in nitrate-limited continuous culture. Journal of Phycology 14, 406–416.

Lohse, L., Helder, W., Epping, E.H.G., Balzer, W., 1998. Recycling of organic matter along a shelf-slope transect across the N.W. European Continental margin (Goban Spur). Progress in Oceanography 42, 77–110.

Lowry, R.K., Loncar, Z.L., Downer, R.M., Kramer, R.N., 1997. OMEX I Project Data Set. CD-ROM electronic publication, British Oceanographic Data Centre, Birkenhead, UK.

Martin, G.P., Delhez, E.J., 1994. 3D turbulence field on the north-western European continental shelf. Tellus 46 A, 98–112.

McGillicuddy Jr., D.J., Robinson, A.R., McCarthy, J.J., 1995. Coupled physical and biological modelling of the spring bloom in the North Atlantic (II): three dimensional bloom and post-bloom processes. Deep-Sea Research 42 (8), 1359–1398.

Middelburg, J.J., Soetaert, K., Herman, P.M.J., 1997. Empirical relationships for use in global diagenetic models. Deep-Sea Research I 44 (2), 327–344.

Millero, F.J., Poisson, A., 1981. International one-atmosphere equation of state of sea-water. Deep-Sea Research 28 A, 625–629.

Oguz, T., Ducklow, H., Malanotte-Rizzoli, P., Tugrul, S., Nezlin, N.P., Unluata, U., 1996. Simulation of annual plankton productivity cycle in the Black sea by a one-dimensional physical–biological model. Journal of Geophysical Research 101, 16585–16599.

Platt, T., Sathyendranath, S., Caverhill, C.M., Lewis, M.R., 1988. Ocean primary production and available light: further algorithms for remote sensing. Deep-Sea Research 35, 855–879.

Prunet, P., Minster, J.-F., Ruiz-Pino, D., 1996. Assimilation of surface data in a one-dimensional physical–biogeochemical model of the surface ocean. 1. Methods and preliminary results. Global Biogeochemical Cycles 10 (1), 111–138.

Radach, G., Moll, A., 1993. Estimation of the variability of production by simulating annual cycles of phytoplankton in the central North sea. Progress in Oceanography 31 (4), 339–419.

Ridderinkhof, H., 1992. On the effects of variability in meteorological forcing on the vertical structure of a stratified watercolumn. Continental Shelf Research 12 (1), 25–36.

Sharples, J., Tett, P., 1994. Modeling the effect of physical variability on the midwater chlorophyll maximum. Journal of Marine Research 52, 219–238.

Smith, S.D., 1988. Coefficients for sea surface wind stress, heat flux and wind profiles as a function of wind speed and temperature. Journal of Geophysical Research 93 (C12), 15467–15472.

Smith, C.L., Richards, K.J., Fasham, M.J.R, 1996. The impact of mesoscale eddies on plankton dynamics in the upper ocean. Deep-Sea Research 43 (11–12), 1807–1832.

Smith, C.L., Tett, P., 2000. A depth-resolving numerical model of physically forced microbiology at the European shelf edge. Journal of Marine Systems 26, 1–36.

Soetaert, K., Herman, P.M.J., Middelburg, J.J., 1996a. A model of early diagenetic processes from the shelf to abyssal depths. Geochimica et Cosmochimica Acta 60 (6), 1019–1040.

Soetaert, K., Herman, P.M.J., Middelburg, J.J., 1996b. Dynamic response of deep-sea sediments to seasonal variations: a model. Limnology and Oceanography 41 (8), 1651–1668.

Soetaert, K., Herman, P.M.J., Middelburg, J.J., 1998. Assessing organic matter mineralisation, degradability and mixing rate in an ocean margin sediment (Northeast Atlantic) by diagenetic modeling. Journal of Marine Research 56, 519–534.

Sokal, R.R., Rohlf, F.J., 1995. BIOMETRY, the principles and practice of statistics in biological research, 3rd edition. Freeman and Company, New York, 887pp.

Tett, P., 1998. Parameterising a microplankton model. Department of Biological Sciences, Napier University, Report ISBN 0 902703 60 9, 60pp.

Tett, P., Droop, M.R., 1988. Cell quota models and planktonic primary production. In: Wimpenny, J.W.T. (Eds.), Handbook of Laboratory Model Systems for Microbial Ecosystems. Vol. 2. C.R.C. Press, Boca Raton, FL, pp. 177–233.

Tett, P., Edwards, A., 1984. Mixing and plankton: an interdisciplinary theme in oceanography. Oceanography and Marine Biology: an Annual Review 22, 99–123.

Thomann, R.V., Mueller, J.A., 1987. Principles of surface water quality modeling and control. Harper and Row, New York, 644pp.

Thorpe, S.A., 1984. The role of bubbles produced by breaking waves in super-saturating the near-surface ocean mixing layer with oxygen. Annales Geophysicae 2 (1), 53–56.

Tusseau, M.-H., Lancelot, C., Martin, J.-M., Tassin, B., 1997. 1-D coupled physical–biological model of the northwestern Mediterranean sea. Deep-Sea Research Part II 44 (3-444), 851–880.

Wallace, D.W.R., Wirick, C.D., 1992. Large air–sea gas fluxes associated with breaking waves. Nature 356, 694–696.

Ward, B.B., Kilpatrick, K.A., Renger, E.H., Eppley, R.W., 1989. Biological nitrogen cycling in the nitracline. Limnology and Oceanography 34 (3), 493–513.

Weiss, R.F., 1970. The solubility of nitrogen, oxygen and argon in water and seawater. Deep-Sea Research I 17, 721–735.